

# EEF2-inactivating toxins engage the NLRP1 inflammasome and promote epithelial barrier disruption upon *Pseudomonas* infection

Miriam Pinilla<sup>1</sup>, Raoul Mazars<sup>1</sup>, Romain Vergé<sup>1</sup>, Leana Gorse<sup>1</sup>, Karin Santoni<sup>1</sup>, Kim Samirah Robinson<sup>2,3</sup>, Gee Ann TOH<sup>2,3</sup>, Laure Prouvensier<sup>4</sup>, Stephen Adonai Leon-Icaza<sup>1</sup>, Audrey Hessel<sup>1</sup>, David Péricat<sup>1</sup>, Marlène Murriss<sup>5,6</sup>, Anthony Henras<sup>7</sup>, Julien Buyck<sup>4</sup>, Céline Cougoule<sup>1</sup>, Emmanuel Ravet<sup>8</sup>, Franklin L. Zhong<sup>2,3</sup>, Rémi Planès<sup>1,8,\*,#,¶</sup>, Etienne Meunier<sup>1,\*,#,¶</sup>

<sup>1</sup> Institute of Pharmacology and Structural Biology (IPBS), University of Toulouse, CNRS, Toulouse, France.

<sup>2</sup> Lee Kong Chian School of Medicine, Nanyang Technological University, 11 Mandalay Road, 308232 Singapore, Singapore;

<sup>3</sup> Skin Research Institute of Singapore (SRIS), 11 Mandalay Road, 308232 Singapore, Singapore.

<sup>4</sup> UFR Medicine and Pharmacy, INSERM U1070, University of Poitiers, Poitiers, France

<sup>5</sup> Department of pneumology, Hospital Larrey, Toulouse, France.

<sup>6</sup> University Hospital of Toulouse, France

<sup>7</sup> Center of Integrative Biology (CBI), University of Toulouse, CNRS, Toulouse, France.

<sup>8</sup> Invivogen, Toulouse, France

\* [r.planes@invivogen.com](mailto:r.planes@invivogen.com) (RP), \* [etienne.meunier@ipbs.fr](mailto:etienne.meunier@ipbs.fr) (EM)

# Current Address: Institute of Pharmacology and Structural Biology (IPBS), University of Toulouse, CNRS, Toulouse, France

¶ These authors equally supervised this work.

## KEY POINTS

- *P. aeruginosa* induces NLRP1-dependent pyroptosis in human corneal and nasal epithelial cells
- *P. aeruginosa* Exotoxin A (EXOA) and other EEF2-inactivating bacterial exotoxins activate the human NLRP1 inflammasome
- EEF2 inactivation promotes ribotoxic stress response and ZAK $\alpha$  kinase-dependent NLRP1 inflammasome activation.
- Bronchial epithelial cells from Cystic Fibrosis patients show extreme sensitivity to ribotoxic stress-dependent NLRP1 inflammasome activation in response to Exotoxin A
- P38 and ZAK $\alpha$  inhibition protects Cystic Fibrosis epithelial cell from EXOA-induced pyroptosis

## ABSTRACT

The intracellular inflammasome complex have been implicated in the maladaptive tissue damage and inflammation observed in chronic *Pseudomonas aeruginosa* infection. Human airway and corneal epithelial cells, which are critically altered during chronic infections mediated by *P. aeruginosa*, specifically express the inflammasome sensor NLRP1. Here, together with a companion study, we report that the NLRP1 inflammasome detects Exotoxin A (EXOA), a ribotoxin released by *P. aeruginosa* Type 2 Secretion System (T2SS) during chronic infection. Mechanistically, EXOA-driven Eukaryotic Elongation Factor 2 (EEF2) ribosylation and covalent inactivation promotes ribotoxic stress and subsequent NLRP1 inflammasome activation, a process shared with other EEF2-inactivating toxins, Diphtheria Toxin and Cholix Toxin. Biochemically, irreversible EEF2 inactivation triggers ribosome stress-associated kinases ZAK $\alpha$ - and P38-dependent NLRP1 phosphorylation and subsequent proteasome-driven functional degradation. Finally, Cystic Fibrosis cells from patients exhibit exacerbated P38 activity and hypersensitivity to EXOA-induced ribotoxic stress-dependent NLRP1 inflammasome activation, a process inhibited by the use of ZAK $\alpha$  inhibitors. Altogether, our results show the importance of *P. aeruginosa* virulence factor EXOA at promoting NLRP1-dependent epithelial damage and identify ZAK $\alpha$  as a critical sensor of virulence-inactivated EEF2.

## INTRODUCTION

*Pseudomonas aeruginosa* is an opportunistic bacterial pathogen that can cause acute and chronic life threatening infections (Qin et al., 2022; Maurice et al., 2018). Due to widespread antibiotic resistance and its adaptation to the airway, skin and cornea of immune-compromised patients (e.g. ciliated dyskinesia, chronic granulomatous diseases, cystic fibrosis), *Pseudomonas aeruginosa* is listed as an important ESKAPE pathogen in the WHO list of microbes of concerns (De Oliveira et al., 2020). *P. aeruginosa* can trigger acute infections thanks to the expression of a Type 3 secretion system (T3SS), which leads to a robust inflammatory reaction mostly mediated by monocytes/macrophages and neutrophils (Qin et al., 2022). However, during chronic infections *P. aeruginosa* switches into a metabolically different state that represses T3SS expression and allows the expression and secretion of a different arsenal of effectors involved in the formation/maintenance of biofilm-like structures, which are extremely resistant to antibiotic treatments (Qin et al., 2022). In addition, the secretion of numerous matrix remodeling factors such as (phospho)lipases, proteases, siderophores, oxidative and toxic molecules strongly contribute to immune response deviation as well as to tissue damages, including epithelial barrier disruption (Qin et al., 2022). In this context, inflammatory mediator analysis from Cystic Fibrosis (CF) patients chronically infected with *P. aeruginosa* highlights an enrichment in inflammasome-derived cytokine IL-1 $\beta$ , suggesting that during the chronic step of *P. aeruginosa* infection one or many inflammasomes might be activated (Bonfield et al., 2012). Given the prominent epithelial cell damage observed in *P. aeruginosa* infected patients, and the poorly addressed function of the epithelial barrier in antibacterial defense, we hypothesized that some epithelial inflammasomes might respond to one or various factors released by *P. aeruginosa* during chronic infections.

Inflammasomes, which mostly belong to the Nod-Like Receptor (NLR) and AIM2-Like Receptor (ALRs) families, are a subset of germline-encoded innate immune sensors that detect and respond to various signs of infections and environmental stresses (Lacey and Miao, 2020). Upon activation, inflammasome-forming sensors assemble a cytosolic supramolecular structure composed of the sensor/receptor, the adaptor protein ASC and the protease Caspase-1. Inflammasome assembly leads to caspase-1-dependent

maturation and release of inflammatory cytokines IL-1 $\beta$  and IL-18 as well as to pyroptosis, a pro-inflammatory form of cell death characterized by gasdermin (D)-driven pore formation and NINJURIN-1-dependent membrane disassembly (Kayagaki et al., 2021; Broz and Dixit, 2016; Lacey and Miao, 2020).

The human NLRP1 inflammasome is notable among other inflammasome sensors because of 1) its epithelia-restricted expression, 2) its divergence from rodent counterparts and 3) its uncommon domain organization. Rare germline mutations and single-nucleotide polymorphisms in NLRP1 are associated with infection sensitivity, skin, corneal and intestinal inflammatory disorders as well as with asthma susceptibility in humans, hence underlying an important function of NLRP1 at triggering an innate immune response in various epithelia (Zhong et al., 2016; Griswold et al., 2022).

A conserved mechanism of NLRP1 inflammasome activation relies on proteasome-driven degradation of the NLRP1 N-terminal autoinhibitory fragment (NT) and the subsequent oligomerization of the released C-terminal fragment (CT), which nucleates the NLRP1 inflammasome assembly. To this regard, recent studies identified human-specific mechanism of NLRP1 inflammasome activation, including the recognition of viral double-stranded RNA, cleavage by 3C and 3CL proteases from rhinovirus and SARS-CoV-2 viruses as well as ZAK $\alpha$  and P38 stress kinase-driven phosphorylation upon exposure to ribosome stressors (UV-B irradiation, anisomycin) (Tsu et al., 2021; Robinson et al., 2020; Griswold et al., 2022; Bauernfried et al., 2021; Robinson et al., 2022; Jenster et al., 2023; Fenini et al., 2018; Planès et al., 2022).

In this study, we discover that in human corneal and nasal epithelial cells, *P. aeruginosa* contributes to barrier disruption by secreting the Eukaryotic Elongation Factor 2 (EEF2)-inactivating toxin Exotoxin A (EXOA), which subsequently triggers assembly of the NLRP1 inflammasome and release of associated IL-1 cytokine as well as pyroptotic cell death. In this process, EXOA-inactivated EEF2 promotes ribotoxic stress response (RSR) and subsequent activation of the stress kinases ZAK $\alpha$  and P38 (Wu et al., 2020; Vind et al., 2020). Subsequently, activated ZAK $\alpha$  and P38 stimulate NLRP1 phosphorylation in its disordered region, functional degradation and activation. Finally, Cystic Fibrosis cells from patients show exacerbated P38 activity and hypersensitivity to EXOA-induced ribotoxic stress-dependent NLRP1 inflammasome activation, a process reverted by the

use of ZAK $\alpha$  inhibitors. Altogether, our results describe the ability of *P. aeruginosa* virulence factor EXOA at promoting NLRP1-dependent tissue damage and identify ZAK $\alpha$  as a critical sensor of bacterial pathogen-driven ribosome inactivation.

# RESULTS

## *P. aeruginosa* infection activates the NLRP1 inflammasome in human corneal and airways epithelial cells

Chronic infections mediated by *P. aeruginosa* can target various sites, including skin (Spernovasilis et al., 2021), cornea (Hazlett, 2005) and airways/lung (Qin et al., 2022) tissues. In certain contexts, *P. aeruginosa* metabolically transitions into a mucoid form that enables biofilm formation. As chronically infected patients exhibit both epithelial alterations and robust IL-1 $\beta$  cytokine levels, we wondered about the contribution of inflammasome response from epithelial compartments during *P. aeruginosa* infection. To mimic *P. aeruginosa* biofilm-like behavior, we relied on a transwell-adapted method that allowed bacteria to grow on top of a 0.4 $\mu$ m porous membrane and where epithelial cells were seeded on the bottom of the wells (**Fig. 1A**). In this context, we analyzed the inflammasome response (IL-1 $\beta$ /IL-18 and cell death) of primary human corneal (pHCECs) and nasal epithelial cells (pHNECs) co-cultured with *P. aeruginosa*. We observed that *P. aeruginosa* triggered robust cell death and IL-1 $\beta$ /IL-18 release both in pHNECs and pHCECs (**Fig. 1A**). Importantly, the use of Z-YVAD, an inhibitor of Caspase-1 activity, underscored that IL-1 $\beta$ /IL-18 release fully depended on Caspase-1 activity while cell death was partly dependent on Caspase-1, Caspase-3 and Caspase-8 (**Fig. 1A**). This suggests that the inflammasome in pHNECs and pHCECs could contribute to IL-1 $\beta$ /IL-18 and cell death in response to extracellular *P. aeruginosa*. In order to determine which inflammasome is involved, we immunoblotted for various inflammasome-forming sensors in those epithelial cells (**Fig. 1B**). Although we failed at detecting NLRP3 expression, we could detect expression of the NLRP1 sensor in addition to the complete inflammasome machinery (ASC, Caspase-1, GSDMD) both in nasal and corneal epithelial cells (**Fig. 1B**) (Robinson et al., 2020; Griswold et al., 2022). Hence, we hypothesized that NLRP1 might be a sensor of extracellular *P. aeruginosa* in the airway and corneal compartments. To address this question, we used our previously described epithelial lung A549-ASC-GFP reporter cell lines in which hNLRP1 construct was stably introduced (Planès et al., 2022). Fluorescence microscopy and quantification of active inflammasome complexes (ASC-GFP<sup>+</sup> puncta/Specks) in co-cultured reporter cells unveiled that *P. aeruginosa* exposure

promoted the formation of inflammasome complexes as well as induced significant cell death specifically in NLRP1-expressing cells (**Fig. 1C**). This suggested that NLRP1 could be a sensor of a yet unknown secreted product by *P. aeruginosa*. To further determine the involvement of NLRP1 in primary cells at responding to extracellular *P. aeruginosa*, we invalidated NLRP1 expression in nasal and corneal epithelial cells by using CRISPR-Cas9 method (**Fig. 1D**). Co-culture of WT and NLRP1-deficient cells with *P. aeruginosa* showed that *NLRP1*<sup>-/-</sup> cells exhibited a defect in cell death (measured by propidium iodide incorporation and LDH release) as well as at releasing IL-1 $\beta$ /IL-18 cytokines (**Fig. 1D, E**). As hNLRP1 inflammasome activation requires ubiquitination and subsequent proteasome-driven functional degradation, which releases the active NLRP1 C-Ter fragment, we next incubated pHCECs with PAO1 or with Val-boro-pro (Vbp), a known chemical activator of the NLRP1 inflammasome, in presence or absence of the proteasome inhibitor bortezomib (**Fig S1A-C**). Measure of the pyroptosis pore forming protein Gasdermin-D processing, hNLRP1 degradation, cell death and IL-1 $\beta$  release in pHCECs showed that proteasome inhibition strongly impaired those processes, hence suggesting that the hNLRP1 inflammasome activation by *P. aeruginosa* occurs in a proteasome-dependent manner in corneal and airway epithelial cells (**Fig S1A-C**).

## EEF2-inactivating Exotoxin A promotes NLRP1 inflammasome response

As the NLRP1 inflammasome responds to a yet to be determined secreted product of *P. aeruginosa*, we next wondered about the identity of this factor. *P. aeruginosa* expresses various secretion systems (T1SS to T6SS) that allows either secreting or injecting various elements (Filloux, 2011, 2022). Using co-cultures of A549-ASC-GFP/NLRP1 reporter cells lines with PAO1 transposon mutants for different secretion systems, we observed that Type-2 Secretion System (T2SS)-deficient PAO1 specifically failed at inducing NLRP1 inflammasome complex assembly (**Fig. 2A**). Among other factors released by PAO1 T2SS are phospholipases (PLCN, PLCH), elastase protease LASB and the Exotoxin A (EXOA) (Liao et al., 2022). Using PAO1 transposon mutants for each of those factors, we observed that only the PAO1 strain that is deficient for Exotoxin A (EXOA) lost the ability of promoting the formation of the NLRP1 inflammasome in our reporter cell



lines (**Fig. 2B**). This suggests that T2SS-secreted EXOA is the major factor with which extracellular *P. aeruginosa* activates the NLRP1 inflammasome in epithelial cells. EXOA is a ribotoxin that irreversibly ribosylates the elongation factor EEF2, which leads to ribosome inactivation (Jørgensen et al., 2005; Armstrong and Merrill, 2004), a process we also observed by determining ribosome polysomes accumulation (marker of alterations in translation machinery) and translation inhibition (puromycin incorporation as a marker of translation efficiency) (**Fig. 2C, D**). In this context, to determine if EXOA ribosylating activity was required for NLRP1 inflammasome response, we exposed reporter cells to recombinant EXOA and the catalytically dead mutant EXOA<sup>H426A</sup>, which is unable to promote EEF2 ribosylation (Roberts and Merrill, 2002) (**Fig. 2E, S2A**). Microscopy observation and quantifications of NLRP1 inflammasome complexes in reporter cells showed that EXOA but not its mutant triggered robust inflammasome formation (**Fig. 2E**). EEF2 ribosylation by EXOA requires the presence of a specific modified form of Histidine 715 on human EEF2, namely Diphthamide (Liu et al., 2004; Ivankovic et al., 2006) (**Fig. S2B**). This unique amino acid arises from the enzymatic modification of Histidine by the so-called Diphthamide enzymes (DPHs) (Liu et al., 2004; Ivankovic et al., 2006). Hence, using our reporter cells, we genetically deleted *DPH1*, which is critical to initiate diphthamide synthesis (**Fig. S2C**). Analysis of NLRP1 inflammasome complexes in response to EXOA showed that *DPH1*-deficient cells failed to assemble an active NLRP1 inflammasome complex (**Fig. S2D**). As control, activation of the NLRP1 inflammasome by the Val-boro-pro (Vbp) molecule was not affected by the removal of *DPH1*, suggesting that EXOA specifically activates the NLRP1 inflammasome by promoting EEF2-ribosylation on the Diphthamide 715 amino acid (**Fig. S2D**). In addition to EXOA, two other bacterial toxins, namely Diphtheria Toxin (*Corynebacterium diphtheriae*) and Cholix toxin (*Vibrio cholera*) (Jørgensen et al., 2008) also promote irreversible ribosylation of human EEF2 on Diphthamide 715 (Liu et al., 2004; Ivankovic et al., 2006; Jørgensen et al., 2005). Hence, to determine if those toxins could also induce NLRP1 inflammasome formation in a similar way than observed with EXOA, we exposed NLRP1 reporter cell lines to those toxins. As for EXOA, we observed that Cholix Toxin and Diphtheria Toxin both triggered robust NLRP1 inflammasome complex assembly in those reporter cells (**Fig. S2D**). Furthermore, NLRP1 inflammasome formation was



abrogated in *DPH1*-deficient A549 in response to Cholix Toxin and Diphtheria Toxin, hence confirming the existence of a shared pathway for EEF2 inactivation by those toxins (**Fig. S2D**).

Finally, exposure of primary WT and NLRP1-deficient corneal epithelial cells to EXOA highlighted an increased protection of *NLRP1*<sup>-/-</sup> cells to cell pyroptosis, suggesting that extracellular *P.aeruginosa*-induced NLRP1 inflammasome response in epithelial cells requires T2SS-secreted EXOA and subsequent EEF2 inactivation (**Fig. 2F**).

### **EEF2 inactivation drives Ribotoxic Stress Response (RSR)-dependent ZAK $\alpha$ and P38 MAPkinase activation and subsequent NLRP1 inflammasome nucleation**

Recent studies unveiled that ribosome inactivation by UV-B as well as the antibiotic anisomycin also promote NLRP1 inflammasome activation in human keratinocytes (Robinson et al., 2022; Jenster et al., 2023; Fenini et al., 2018). Furthermore, this mode of activation engages the MAP3K ZAK $\alpha$  and the effector P38 $\alpha/\beta$  kinases (Robinson et al., 2022; Jenster et al., 2023; Fenini et al., 2018). Thus we wondered if EXOA-driven EEF2a irreversible inactivation and subsequent NLRP1 inflammasome formation might also engages a similar pathway. We generated ZAK $\alpha$ -deficient reporter cell lines and measured their ability to promote activation of the MAPK stress kinases in response to EXOA exposure (**Fig. 3A, S3A**). We observed that EXOA, but not its inactive mutant EXOA<sup>H426A</sup>, strongly induced P38 and JNK stress kinase phosphorylation, a process that disappeared in absence of ZAK $\alpha$  (**Fig. 3A, S3A**). Further analysis of NLRP1 inflammasome formation using fluorescence microscopy highlighted that ZAK $\alpha$  deficiency completely abrogated assembly of the NLRP1 inflammasome and cell death in response to EXOA (**Fig. 3B**). To further analyze if ZAK $\alpha$  and its downstream effectors P38 were important for NLRP1 inflammasome formation, we genetically deleted P38 $\alpha$ , P38 $\beta$  or both P38 $\alpha/\beta$  in reporter cells and quantified inflammasome assembly in response to EXOA (**Fig. 3C, S3B**). We observed that single deletion for P38 $\alpha$  or P38 $\beta$  did not strongly modify inflammasome assembly whereas combined deficiency for P38 $\alpha/\beta$  led to a robust defect in NLRP1 inflammasome formation upon EXOA exposure (**Fig. 3C**). This suggests that ZAK $\alpha$ - and ZAK $\alpha$ -activated P38 kinases contribute to NLRP1 inflammasome response to EXOA.

ZAK $\alpha$  and P38-driven phosphorylation of Serine and Threonines in the NLRP1 disordered region has been recently shown to promote NLRP1 inflammasome activation upon UV-B-driven ribosome collision (Robinson et al., 2022). Here, using NLRP1 constructs mutated for either phosphorylation site 1 (<sup>110</sup>TST<sup>112</sup>) or site 2 (<sup>178</sup>TST<sup>180</sup>), we observed that EXOA was unable to trigger assembly of the NLRP1 inflammasome in reporter cells (Fig. 3D, E). To the contrary, Vbp- and SARS-CoV-2-induced NLRP1 inflammasome assembly was fully efficient in cells complemented with either construct or in ZAK $\alpha$ -deficient cells (Fig. 3D, E, S3C). All in one, those results suggest that ZAK $\alpha$ - and P38-targeted NLRP1 site 1 and 2 is required for efficient inflammasome assembly in response to EXOA but not during Vbp or SARS-CoV-2 exposure.

### **Cystic fibrosis airway epithelial cells show exacerbated sensitivity to EXOA-driven cell death, which is reversed by ZAK $\alpha$ inhibition**

Next we investigated the role of EXOA-driven pyroptosis in a patho-physiological model of *P. aeruginosa* infection. In addition to causing corneal infections, *P. aeruginosa* is well known to establish life-threatening infection in airways and lungs of Cystic Fibrosis (CF) patients. Due to defective mucus production and clearance (Veit et al., 2016), the airway of CF patients favor chronic *P. aeruginosa* infections. Collaborating with the Hospital of Toulouse, we obtained nasal brushes from healthy and Cystic fibrosis patients carrying the  $\Delta$ F508 mutation in the CFTR ( $\Delta$ F508 / 4005+1G>A and  $\Delta$ F508 / N1303K, respectively referred in the text and figure legends as CF donors 1 and 2) (Fig. S4A). CF patients have been described to express very high basal and inducible P38 kinase activation (Raia et al., 2005; Bérubé et al., 2010), a phenotype we could confirm by exposing or not those cells to EXOA (Fig. 4A). Given the importance of P38 kinases at promoting EXOA-dependent NLRP1 inflammasome response, we next measured the ability of healthy and CF nasal cells to undergo EXOA-dependent cell death. Propidium incorporation measure in healthy and CF nasal cells showed that EXOA-driven cell death was exacerbated in CF nasal cells, a process that was reduced by the use of P38 inhibitor SB203580 (Fig. 4B). Further experiments also showed that ZAK $\alpha$  inhibition (PLX4720) even further inhibited EXOA-driven cell death, Gasdermin D cleavage and IL-18 release both in healthy and CF nasal cells (Fig. 4C-F, S4B). Such process was conserved with the

ribotoxic antibiotic anisomycin but not in response to Vbp where nasal cells from healthy and CF patients responded similarly, hence suggesting that P38 pre-activation in CF patients specifically sensitive them to ribotoxic stress-driven NLRP1 response, a process that may contribute to *P. aeruginosa*-driven epithelial barrier disruption (**Fig. 4D-F, S4B**). Altogether, our results suggest that the ZAK $\alpha$ /NLRP1 axis contributes to exacerbated epithelial barrier destabilization upon EXOA-inactivated EEf2 exposure.

## DISCUSSION

Chronic infections of multiple organs mediated by *P. aeruginosa* are a major source of epithelium damage and inflammatory exacerbations. Due to the lack of robust and relevant models of study as well as its remarkable adaptation to specific environments, the impact of chronic infections mediated by *P. aeruginosa* on host epithelial integrity has long been hard to address. Here, our findings and those from the Zhong group (companion manuscript) that the T2SS-released Exotoxin A, and its relatives Cholix and Diphtheria Toxins, trigger activation of the human NLRP1 inflammasome in skin keratinocytes, corneal and airway epithelial cells, three important sites of *P. aeruginosa* chronic infections. This process exemplifies a novel biochemical pathway by which epithelial organs detect bacterial virulence factors.

Although major research studies unveiled that upon acute infection, *P. aeruginosa* T3SS allows both activation of the NLRC4 and NLRP3 inflammasomes in rodent as well as in human macrophage and neutrophil models (Sutterwala et al., 2007; Faure et al., 2014; Franchi et al., 2007; Miao et al., 2008; Deng et al., 2015; Balakrishnan et al., 2018; Santoni et al., 2022a; Ryu et al., 2016), chronic infections mediated by this pathogen is associated with a downregulation of T3SS in favor a biofilm phenotype, where EXOA is strongly produced and released. To this regard, our observation that EXOA-driven ribotoxic stress contributes to exacerbated tissue damage and inflammation strongly correlate with earlier studies which showed that EXOA-deficient bacteria triggered lower tissue damages during infections of human and mice (Michalska and Wolf, 2015; Pillar and Hobden, 2002). Even though the RSR-driven NLRP1 inflammasome path is not conserved among rodents and humans, ZAK $\alpha$ -driven RSR constitutes a shared process between both species, which suggests that evolution selected ZAK $\alpha$  as a versatile stress

sensor. To the contrary, for yet to be determined reasons, human-specific evolution has linked RSR to NLRP1 inflammasome response in epithelia, which suggests a specific importance for such selection.

A caveat of this work mostly relies on the yet to be determined identification of Ubiquitin ligases that promote NLRP1 functional degradation upon ZAK $\alpha$ -driven phosphorylation, which is currently under investigations. The sensitivity of NLRP1 activation to the Nedd8 inhibitor MLN4924 suggests that Nedd8-driven Cullin ligase activation is of major importance in this process (Jenster et al., 2023; Robinson et al., 2022). Among the broad family of Cullin ligases, Cull1 and 2 were found to target phosphorylated proteins for Ubiquitination and subsequent degradation (Chen et al., 2021). Should one of those Ubiquitin ligase complex be involved constitutes an attractive hypothesis to pursue.

In addition to UVB, Chikungunya virus, the antibiotic anisomycin and the fungal toxin DON (Fenini et al., 2018; Jenster et al., 2023; Robinson et al., 2022), our work, along the one from Zhong lab, unveils the critical involvement of the NLRP1 inflammasome upon infections mediated by various bacterial pathogens, including *C. diphtheria* and *P. aeruginosa*. To this regard, patients developing Cystic fibrosis (CF) show exacerbated inflammation and tissues damages upon chronic infection with *P. aeruginosa*. Specific studies highlighted that stress-activated kinases P38 and JNK were over activated in CF-derived cells from patients (Bérubé et al., 2010; Raia et al., 2005). Although various hypothesis were developed to explain such dysregulation in CF patients, no study, including ours, could unveil the critical molecular and biochemical mechanisms engaged, which warrants for further investigations. However, our findings that in this context, EXOA- but also other RSR inducers specifically triggered an exacerbated cell death response suggest that targeting ZAK $\alpha$  and/or P38 kinases in *P. aeruginosa*-infected patients might constitute a good host-targeted approach in order to limit epithelial damages complementary to the current antibiotic and CFTR modulator strategy used (Kaftrio | European Medicines Agency).

Finally, it is long been noted that host EEF2 (and EEF1) is targeted by a variety of exotoxins from different unrelated bacterial species. Indeed, EEF2 is highly conserved in all eukaryotic species, all expressing a specific diphtamide amino acid. In this context, yeasts as well as mammals are similarly targeted by EXOA and relative toxins, which

underlines the outstanding adaptation of *P. aeruginosa* to its environment but also raises the question of the specific species where EXOA holds the most prevalent/potent role for bacterial development/survival. Another key question lies on the recent identification DPH1 and 2 deficient patients (Urreizti et al., 2020; Nakajima et al., 2018; Hawer et al., 2020). If those deficiencies might actually confer a selective advantage or not to *C. diphtheria*, *V. cholera* or *P. aeruginosa* infections will constitute an exciting field of investigations, as previously observed for HIV- or-malaria-resisting patients (Samson et al., 1996; Allison, 1954) or recently highlighted for *Yersinia pestis*-shaped selection/evolution of the inflammasome-forming sensor PYRIN (Park et al., 2020). All in one, our results describe the critical role of ZAK $\alpha$ -driven NLRP1 inflammasome response and epithelial disruption in response to the pathogen *P. aeruginosa*, and exemplify its deleterious potential in CF pathogenesis.

## ACKNOWLEDGMENTS

We are extremely grateful to patients and their families for their willingness of participating to this study. Authors also warmly acknowledge Y. Rombouts, L. Boyer, T. Henry, M. Tiraby and all lab members for their outstanding advices and support on this project. This project was supported by the ATIP-Avenir program (to EM), FRM “Amorçage Jeunes Equipes” (AJE20151034460 to EM), the Agence Nationale de la Recherche (ANR Psicopak to EM), the ANRS-MIE (to EM), the ERC (StG INFLAME 804249 to EM), the European Society of Clinical Microbiology and Infectious Diseases (ESCMID, to RP), Invivogen-CIFRE PhD grant (to MP), Vaincre La Mucoviscidose (VLM) and Region Occitanie (GRAINE) grants to CC. The funders had no role in study design, data collection and analysis, decision to publish, or preparation of the manuscript.

## MATERIAL AND METHODS

**Ethic statements:** Patient data and tissue collection was performed in agreement with European Network of Research Ethics Committees and French ethic law. The ethical committee, according to the Medical Research Involving Human Subjects Act, reviewed and approved the study. Human tissue was provided by the University Hospital of Toulouse (France) and CNRS (agreements CHU 19 244 C and CNRS 205782). All patients involved in this study declared to consent to scientific use of the material; patients can withdraw their consent at any time, leading to the prompt disposal of their tissue and any derived material.

### Reagent used in the study

Antibody	Catalog Reference	Provider
Rabbit anti-ZAK antibody 1: 1000	A301-993A	Bethyl Laboratories
P38 MAPK antibody 1: 1000	9212S	Cell signaling
Phospho-P38 MAPK (Thr180/Tyr182) (D3F9) XPRabbit mAb 1: 1000	4511S	Cell signaling
JNK1 Rabbit anti-Human Polyclonal 1: 1000	44690G	Invitrogen
Phospho-SAPK/JNK (Thr183/Tyr185) (81E11) Rabbit mAb 1: 1000	4668S	Cell signaling
Anti NLRP1 1:200	679802	Biolegend
Anti NLRP1 (N-terminal) 1: 1000	AF6788-SP;RRID: AB_2916167	R&D systems
Anti- NLRP1 (C-terminal), 1: 1000	ab36852;RRID: AB_776633	abcam
anti-Sheep igG HRP (1/4000)	HAF016;RRID: AB_562591	R&D

Goat-anti-rabbit IgG (H+L), HRP conjugate (1/5000)	R-05072-500;RRID: AB_10719218	Advansta
GSDMDC1 antibody 1: 1000	NBP2-33422	biotechne
Anti-Puromycin Antibody, clone 12D10	MABE343	Sigma
EEF2 antibody (1:1000)	2332S	Cell signaling
DPH1 antibody (1:1000)	# H00001801-M02	ThermoFisher scientific
Anti-alpha Tubulin antibody 1: 1000	ab4074	Abcam
Streptavidin - HRP	434323	ThermoFisher scientific
<b>Reagents</b>	<b>Catalog Reference</b>	<b>Provider</b>
Transwell	140620	ThermoFisher scientific
NAD <sup>+</sup> , Biotin-Labeled	80610	BPSBioscience
Pseudomonas exotoxin A 0.5 mg	P0184-.5MG	sigma
Inactive Exotoxin A	N.A.	Creative Diagnostics
Diphtheria Toxin	D0564-1MG	Sigma
Cholix toxin	This study	This study
Anisomycin	SE-S7409-10MG	selleck
Talabostat (Vbp)	tlrl-vbp-10	invivoGen
PhoSTOP	4906845001	sigma/Roche
cOmplete, Mini, EDTA-free Protease Inhibitor Cocktail	4693159001	Sigma/roche
Lipofectamine LTX	15338030	Invitrogen
Puromycin Dihydrochloride	A1113803	gibco



Molecular Probes SYTOX Green Nucleic Acid Stain	S7020	Thermofisher
Propidium iodide	P1304MP	Thermofisher
Nate	lyec-nate	Invivogen
<b>Critical commercial assays</b>	<b>Catalog Reference</b>	<b>Provider</b>
Human total IL-18 duo set	DY318-05	R&D
Cyquant LDH	C20301	Thermofisher
Human IL-1beta	88-7261-77	Thermofisher
Q5 Site-Directed Mutagenesis Kit Protocol	E0554	NEB
<b>Chemicals</b>	<b>Catalog Reference</b>	<b>Provider</b>
ZAK inhibitor (PLX-4720) 10μM	HY-51424	Med Chem Express
P38 inhibitor SB 203580 10μM	HY-10256	Med Chem Express
Caspase-1 inhibitor - Ac-YVAD-cmk 20μM	inh-yvad	invivogen
Z-VAD-FMK 20μM	vad-tlrl:	invivogen
Caspase-3/7 inhibitor ZDEVD-FMK 20μM	S7312	Selleck
Caspase-8 inhibitor - Z-IETD-FMK	inh-ietd	invivogen
Bortezomib 1μM	S1013	selleck
Cycloheximide (CHX)	C4859-1ML	Sigma
<b>Human Primary Nasal Epithelial cells</b>	<b>Catalog Reference</b>	<b>Provider</b>

Tryple Express Enzyme (1X), no phenol red	10718463	Fisher Scientific
Nutragen Type I Collagen Solution, 6 mg/ml (Bovine)	5010-50ML	Advanced Biomatrix
Sputolysin	560000-1SET	Sigma
PneumaCult-Ex Plus Medium	05040	Stem cell
Costar 6.5 mm Transwell, 0.4 µm Pore Polyester Membrane Inserts	38024	Stem cell
<b>Human Primary Corneal epithelial cells</b>	<b>Catalog Reference</b>	<b>Provider</b>
Human Corneal Epithelial Cell Growth Medium	221-500	Tebu-bio
Human corneal epithelial cells	630-05a	Tebu-bio
<b>Cell lines</b>	<b>Catalog Reference</b>	<b>Provider</b>
A549 ASC GFP NLRP1	a549-ascg-nlrp1	Invivogen
A549 ASC GFP	a549-ascg	Invivogen
A549 ASC GFP NLRP1/ACE2	a549-ascov2-nlrp1	Invivogen
A549 ASC GFP ACE2	a549-ascov2	Invivogen
<b>Recombinant DNA</b>	<b>Catalog Reference</b>	<b>Provider</b>
hNLRP1 gene	puno1-hnalp1a	Invivogen

## Cell culture

A549 cells were maintained in Dulbecco's modified Eagle's medium (DMEM, Gibco) supplemented with 10% heat-inactivated fetal bovine serum (FBS), 1% penicillin-streptomycin, and 1% L-glutamine at 37°C 5% CO<sub>2</sub>. Primary Human Corneal epithelial cells were maintained in Human Corneal Epithelial Cell Growth Medium (Tebu-bio) at 37°C 5% CO<sub>2</sub>.

Regarding primary Human Nasal Epithelial Cells (pHNECs), patients' pHNECs were collected on superior turbinates using smear brushes at the Hospital of Toulouse, France.

After brushing back cells in collection medium, centrifugation was performed for 5 min 400g at 4°C. Pellet was resuspended in 4 ml TrypLE express (GIBCO) + 20µl Sputolysin (200X) and incubated at 37°C for 5 minutes to disrupt mucus. TrypLE was diluted with 4 ml of Advanced DMEM F12- .

Pellet was recovered after centrifugation and culture was continued in the expansion medium Pneumacult). After a week of proliferation, basal cells were counted and seeded onto collagen-coated (0.03mg/mL) and maintained in Pneumacult Ex Plus Medium (StemCell) at 37°C 5% CO<sub>2</sub>.

### Cell Stimulations

Otherwise specified, cells were plated one day before stimulation in 12-well plates at 200 000 cells per well in 1mL of DMEM, 10% FCS, 1% PS.

Medium was changed to OPTIMEM and cells were preincubated or not with the indicated inhibitors during 1 hour.

The pHNE cells were seeded the day before the stimulation in 12-well plates at 200 000 cells per well in 1mL of pneumacult medium. Cell's medium was changed to OPTIMEM and cells were treated or not with the indicated inhibitors during 1 hour.

The pHCE cells were seeded the day before the stimulation in 12-well plates at 10 000 cells per well in 1 mL of corneal epithelial cell growth medium. Medium of the cells was changed to OPTIMEM and cells were treated or not with the indicated inhibitors during 1 hour.

All cells were treated with the indicated concentration of Exotoxin A (EXOA, 10 ng/mL to 1µg/mL), anisomycin (1µM) or with Val-boroPro (15µM) for indicated times.

SARS-CoV-2 (BetaCoV/France/IDF0372/2020 isolate) experiments were performed in BSL-3 environment as described in (Planès et al., 2022).

Briefly, 250,000 A549<sup>ASC-GFP/NLRP1/ACE2</sup>, genetically invalidated or not for ZAKα, were infected for 24 hours with BetaCoV/France/IDF0372/2020 strain at indicated MOI in DMEM supplemented with 10mM Hepes, 1% penicillin-streptomycin and 1% L-Glutamine for 1h at 37°C.

## Transwell infections

A549 cells, expressing or not NLRP1, along with the ASC-GFP reporter, were plated in 24 well plates at  $2 \times 10^5$  cells per well one day before experiment. The following day, cell culture media was replaced by 600  $\mu$ L of OPTI MEM per wells. Cells were placed in co-culture with Pao1 bacteria WT or mutant (as indicated) at MOI of 10, in 100  $\mu$ L of OPTI MEM separated by a semi-permeable transwell insert (0.3 $\mu$ m). After 18 hrs of co-culture, transwell inserts containing bacteria were removed and ASC-speck formation in A549 cell was analyzed. Images were acquired using EVOS M700 microscope.

## Bacterial growth and mutants

*P. aeruginosa* strains (PAO1) and their isogenic mutants were grown in Luria Broth (LB) medium overnight at 37°C with constant agitation. The following day, bacteria were sub-cultured by diluting overnight culture 1:25 and grew until reaching an optical density (OD) O.D.600 of 0.6 – 0.8.

PAO1 and its transposon mutants were obtained from two-allele transposon library (Jacobs et al., 2003).

Name	Exact	Location	ORF	Gene Abbrev.
PW3079	+	phoAwp05q1C05	PA1148	toxA (EXOA)
PW2538	+	phoAwp03q1H07	PA0844	plcH (PLCH)
PW6586	+	phoAwp08q2E01	PA3319	plcN (PLCN)
PW6221	+	lacZwp03q2D06	PA3105	xcpQ (T2SS)
PW7302	+	phoAbp02q4F10	PA3724	LasB (LASB)
PW4017	+	lacZbp02q3F02	PA1706	pcrV (T3SS)
PW10311	+	lacZbp02q1B09	PA5503	ABC transporter (T1SS)

Specific deletion of xcpQ (T2SS) and toxA (EXOA) genes was achieved as described previously in (Santoni et al., 2022b). Briefly, pEXG2 suicide vector containing 700-bp sequences of the flanking regions of the selected gene was directly inserted into competent SM10 $\lambda$ pir (Mix&Go competent cells, Zymo Research Corporation) and

subsequently selected on LB-Agar supplemented with 50 µg/mL kanamycin /15 µg/mL gentamicin. After sequencing resulting clones were mated with PAO1 strains, 4H/37°C. Mated bacteria were plated on 15 µg/mL gentamicin and 20 µg/mL Irgasan LB-Agar plates in order to selectively remove E.coli SM10 strains. Next day, 5-10 clones were grown for 4h in LB and streaked on 5% sucrose LB plates overnight at 30°C. PAO1 clones were then checked by PCR for mutations.

Name	Sequence	Targeted Gene
607_JB_PA_m_toxA_R1 Fw	CCCAGTCTCGAGGTCGACGGTATCGATAAGCTTGAT ATCGAATTCggccgacggcggc	toxA
608_JB_PA_m_toxA_R1 Rv	tcgcatgcacctgacacccgaggacctaagtaactgccgc	toxA
609_JB_PA_m_toxA_R2 Fw	ggcagttacttcaggtcctcggtgtcaggtgcatcgc	toxA
610_JB_PA_m_toxA_R2 Rv	CTGGAGCTCCACCGCGGTGGCGGCCGCTCTAGAAC TAGTGGATCCagccattgttcgacgaataaagccacc	toxA
611_JB_PA_m_toxA_Check R1	gaagtactcaacgggtgatcccc	toxA
612_JB_PA_m_toxA_Check R2	cgttccgcaacgcttgaagt	toxA
EM019-xcpQ R1 Fw	ttccacacattatacgagccggaagcataaatgtaaagcaagcttACGAT AAAGACCAGGAGTGATGTATTGCC	XcpQ
EM020-xcpQ R1 Rv	CGCCGTTATTCCGTCATCAGCAAAGGCTGGGACATC GG	XcpQ
EM021-xcpQ R3 Fw	ACCCGATGTCCCAGCCTTTGCTGATGACGGAATAAC GGCGCC	XcpQ
EM022-xcpQ R3 Rv	ggaaattaattaaggtaccgaattcgagctcgagccggggatccACGC CTGGTTCGTGGC	XcpQ

EM023-xcpQ R1 check	CCCGGCCAGTCACACCTATTGAT	XcpQ
EM024-xcpQ R3 check	AGTGCTTGCCGACAACGACC	XcpQ

## Cell death assays

Cell lysis was measured by quantification of the lactate dehydrogenase (LDH) release into the cell supernatant using LDH CyQUANT kit (Thermofisher). Briefly, 50 µL cell's supernatants were incubated with 50 µL LDH substrate and incubated for 30 min at room temperature protected from light.. The enzymatic reaction was stopped by adding 50 µL of stop solution. Maximal cell death was determined with whole cell lysates from unstimulated cells incubated with 1% Triton X-100

**Plasma membrane permeabilization assays were performed using propidium iodide incorporation.** Cells were plated at density of  $1 \times 10^5$  per well in Black/Clear 96-well Plates in OPTI-MEM culture medium supplemented with Propidium Iodide dye (1µg/mL) and infected/treated as mentioned in figure legends. Red fluorescence is measured in real-time using a Clariostar plate reader equipped with a 37°C cell incubator or using an EVOS Flouid microscope (Invitrogen). Maximal cell death was determined with whole cell lysates from unstimulated cells incubated with 1% Triton X-100.

## Cytokine quantification

Cytokines secretions was quantified by ELISA kits, according to the manufacturer's instructions, IL-1B (Thermo Fisher Scientific, (88-7261-77), IL-18 (Biotechne, DY318-05).

## Sample preparation for immunoblot

At the end of the experiment, cell' supernatant was collected and soluble proteins were precipitated using trichloroacetic acid (TCA) as described previously (Santoni et al., 2022b). Precipitated pellet was then resuspended in 50 uL of RIPA buffer (150 mM NaCl, 50 mM Tris-HCl, 1% Triton X-100, 0.5% Na-deoxycholate) supplemented with protease inhibitor cocktail (Roche). Adherent cells were lysed in 50 uL of RIPA buffer supplemented

with protease inhibitor cocktail (Roche). Cell lysate and cell supernatant were homogenized by pipetting up and down ten times and supplemented with laemli buffer (1X final) before boiling sample for 10 min at 95°C.

## **Immunoblot**

Cell lysates were separated by denaturing SDS-PAGE and transferred on PVDF membrane. After transfer, the membrane is saturated 1h at room temperature in TBS-T (Tris 10 mM pH 8, NaCl 150 mM, Tween 20 0.05%) containing 5% BSA. Then, the membrane is incubated overnight at 4°C with the different primary antibodies, under agitation. After 3 washes with TBS-T, the membrane is further incubated with the secondary antibodies coupled with the peroxidase enzyme HRP (horseradish peroxidase) for 1 hour at room temperature and under agitation. Then membranes are washed 3 times with TBS-T. ECL revelation kit (Advansta) was used as a substrate to reveal HRP activity and membranes are imaged using ChemiDoc Imaging System (BioRad). The primary antibodies and secondary antibody used are listed in Reagent table.

## **Phosphoblots**

At the end of the experiment, cell' supernatant was discarded and adherent cells were lysed in 50 uL of RIPA buffer (150 mM NaCl, 50 mM Tris-HCl, 1% Triton X-100, 0.5% Na-deoxycholate) supplemented with protease inhibitor cocktail (Roche) and phosphatase inhibitors cocktails (Roche). Collected cell lysate was homogenized by pipetting up and down ten times and supplemented with laemli buffer before boiling for 10 min at 95°C. Cell lysates were then separated by SDS-PAGE and handled as described in the immunoblot section.

## **Puromycin incorporation**

The day before the stimulation A549 ASC-GFP expressing or not NLRP1 were seeded in 12-well plates at 200 000 cells in 1mL of DMEM 10% FCS 1% PS. Cells were treated with exotoxin A (10 ng/mL) for indicated times. 30 min before the end of the treatment puromycin antibiotic was added in cell medium at 1ug/mL final. Following puromycin



incubation, supernatant was discarded and adherent cells were prepared for immunoblot as described in the immunoblot section. Puromycin incorporation was revealed using the following antibody Anti-Puromycin Antibody (clone 12D10 MABE343).

**Polysomes Profiling.** Sucrose gradient preparation. Five sucrose solutions containing 10 %, 20 %, 30 %, 40 % and 50 % sucrose (w/v) were prepared in TMK buffer (20 mM Tris-HCl pH 7.4, 10 mM MgCl<sub>2</sub>, 50 mM KCl). Layers of 2.1 mL of each solution were successively poured into 12.5 mL polyallomer tubes (Beckman-Coulter, Cat. # 331372), starting from the most concentrated solution (50 %) at the bottom of the tubes to the least concentrated solution (10 %) at the top. Each layer was frozen in liquid nitrogen before pouring the following one. Frozen gradients were stored at - 80 °C and slowly thawed overnight at 4°C before use. Extract preparation. A549 cells were grown to 70% confluency and then treated or not with exotoxin A (10 ng/mL) for indicated times. Following this treatment, cells were incubated with Cycloheximide (CHX, 100 ug/mL) for 15 min at 37°C. Following treatment, cells were rinsed twice with PBS and treated with 1mL of trypsin (0,25%) for 5 min at 37°C. Trypsin was diluted with DMEM medium containing 100 ug/mL of CHX. Cells were mixed up and down and counted to adjust the final resuspension volume in each condition. Cells were centrifuged at 1200 rpm (300g) for 5 min at 4°C. The cell pellet was washed with ice-cold PBS containing 100ug/mL of CHX. Cells were centrifuged at 1200 rpm (300g) for 5 min at 4°C. Supernatants were aspirated and gently lysed in lysis buffer (20 mM Tris-Cl [pH 8], 150 mM KCl, 15 mM MgCl<sub>2</sub>, 1% Triton X-100, 1mM DTT, 100ug/mL CHX, EDTA-free and Protease inhibitor cocktail. Samples were incubated on ice for 20 min and centrifuge at 1000 g for 5 min at 4 °C min and supernatant corresponding to the cytosolic fraction of the cells were collected into a 1.5 mL tube. Samples were further centrifugated at 10 000 g for 5 min at 4°C to clarify the cytoplasmic extract. Extracts were quantified by measuring absorbance at 260 nm using Nanodrop.

**Extracts loading, gradient centrifugation and collection.** Normalized amounts of extracts were loaded on 10–50% sucrose gradients, and then centrifuged at 260,800 x g for 2.5 h at 4°C in an Optima L-100XP ultracentrifuge (Beckman–Coulter) using the

SW41Ti rotor with brake. Following centrifugation, fractions were collected using a Foxy R1 gradient collector (Teledyne Isco) driven by PeakTrak software (Version 1.10, Isco Inc.). The  $A_{254}$  was measured during collection with a UA-6 UV/VIS DETECTOR (Teledyne Isco). The final polysome profiles were generated in Excel from .txt files extracted from PeakTrak software.

### EEF2 ribosylation assays

Cell lysates from A549 were prepared by suspending one pellet of  $1 \cdot 10^6$  A549 cells in 100  $\mu$ L of RIPA buffer. For in-vitro ADP-ribosylation assays, reactions were performed in Eppendorf tube by mixing 50  $\mu$ L of whole cell lysate with 100  $\mu$ L of ADP-ribosylation buffer [20 mM Tris-HCl (pH 7.4), 150 mM NaCl and 1 mM DTT] supplemented with NAD<sup>+</sup> Biotin-Labeled (BPSBioscience) at 50  $\mu$ M final, in presence or absence of recombinant EXOA protein (100 ng). Reaction was left for 1h at 25°C. 20  $\mu$ L of the reaction was analyzed by SDS-PAGE followed by Western blotting as described in the immunoblot section. Membranes were first subjected to EEF2 detection (using anti-EEF2 followed by HRP-conjugated secondary antibody), then membranes were stripped, and ADP-ribosylation was detected by monitoring the incorporation of the NAD<sup>+</sup> Biotin-Labeled probe using streptavidin-HRP-conjugate.

### Generation of mutations in NLRP1 gene

To generate NLRP1 gene mutated for each phosphorylation sites (site 1 (<sup>110</sup>TST<sup>112</sup>) or site 2 (<sup>178</sup>TST<sup>180</sup>)) Threonines and Serines were substituted with Alanine in the human NLRP1 gene (isoform 1) by site-directed mutagenesis using Q5 site-directed mutagenesis Kit Protocol (E0554) according to the manufacturer's instructions. Following primers were used:

Primer FWD site 1 (3406-3414)	cgccGCAGTGCTAATGCCCTGG	68°C
Primer RV site 1	gcggcGGGTTGGCTGGGAGACCC	68°C
Primer FWD site 2 (3604-3612)	cgcaGCAGTGCTGGGGAGCTGG	72°C

Primer RV site 2	gctgcGGGGGCGTTGGGTGACTC	72°C
------------------	-------------------------	------

599

## 600 **Cell transfection**

601 The day prior to the transfection, A549 cells were plated in 6 well plate at  $2 \times 10^5$  cells per  
 602 well in 1ml of DMEM complete medium. The following day, cells were incubated with Nate  
 603 1X (Invivogen) for 30 min. 1  $\mu$ g of NLRP1 plasmids (pLvB72 hNLRP1, pLvB72  
 604 hNLRP1(3604-3612), pLvB72 hNLRP1 (3406-3414) were transfected using lipofectamine  
 605 LTX and PLUS reagent according to the manufacturer's instructions (Invitrogen).  
 606 Transfected cells were incubated for 48 h before further treatments.

607

## 608 **Cholix toxin production**

609 Recombinant cholix toxin (ChxA) was produced using an adapted methodology from  
 610 (Ogura et al., 2011). Briefly, BL21 (DE3) *E. coli* expressing chxA with a N-terminus  
 611 hexahistidine-MBP-tag were harvested and bacteria were lysed by sonication on ice.  
 612 Recombinant cholix toxin was first purified on nickel metal affinity chromatography  
 613 (Takara) and subsequent TEV protease-mediated 6His-MBP tag removal at 4°C/Over  
 614 Night (ON). Then, a second nickel metal affinity chromatography allowed harvesting  
 615 Cholix toxin in the flow-through fraction.

616

## 617 **Genetic invalidations**

618 Genetic invalidation of NLRP1 in primary Human Nasal Epithelial Cells (pHNEs) and  
 619 primary Human Corneal Epithelial Cells (pHCECs) was achieved by using  
 620 Ribonucleoprotein (RNP) technic and nucleofection as described previously (Planès et  
 621 al., 2022). RNP mixes containing Cas9 protein (90pmoles, 1081059, IDT), gRNA  
 622 (450pmoles) and electroporation enhancer (1 $\mu$ L/Mix, 1075916, IDT) were electroporated  
 623 using the Neon transfection system (Life Technologies) in T Buffer (Life Technologies).  
 624 Settings were the following: 1900 V Voltage, 10 Width, 1 Pulse, 20ms.

625 Efficient NLRP1 targeting sgRNA sequence was provided by FL. Zhong (5'  
 626 GATAGCCCGAGTGCATCGG 3') (Robinson et al., 2022).

627 Regarding genetic invalidation of P38 isoforms and ZAK $\alpha$ , A549 cells were transduced  
 628 with LentiCRISPR-V2 vectors containing sgRNA guides against DPH1, P38 isoforms and

ZAK $\alpha$ . 48h after transduction, cells were selected during 2 weeks and puromycin double resistant cells were used in functional assays. A second round of lentiviral infection with lenti-Blasticidin-sgP38 $\beta$  in single KO cells for P38 $\alpha$  achieved generation of double KO cells for P38 $\alpha$  and P38 $\beta$ . Cells were subsequently selected in blasticidin antibiotic before checking genetic invalidation by immunoblotting.

Guides used to generate genetic invalidation

P38 alpha (MAPK14)	5' AGGAGAGGCCACGTTCTAC 3'	FWD
P38 beta (MAPK11)	5' GCCCTCGCGCCGGCTTCTAC 3'	FWD
ZAKalpha (MAP3K20)	5' TGTATGGTTATGGAACCGAG 3'	FWD
Dph1	5' GTTCACGGAGGCCGAAGTGA 3'	FWD
CD8	5' TCGTGGCTCTTCCAGCCGCG 3'	FWD

## Analysis

Prism 8.0a (GraphPad Software, Inc) was used to perform statistical analysis. All relevant informations are included directly in figure legends. Otherwise written, data are reported as mean with SEM. Regarding comparison between two groups, T-test with Bonferroni correction was chosen and multiple group comparisons was analyzed by using Two-way Anova with multiple comparisons test. P values are shown in figures and are linked to the following meaning; NS non-significant and Significance is specified as \* $p \leq 0.05$ ; \*\* $p \leq 0.01$ , \*\*\* $p \leq 0.001$ .

# 649 **FIGURE LEGENDS**

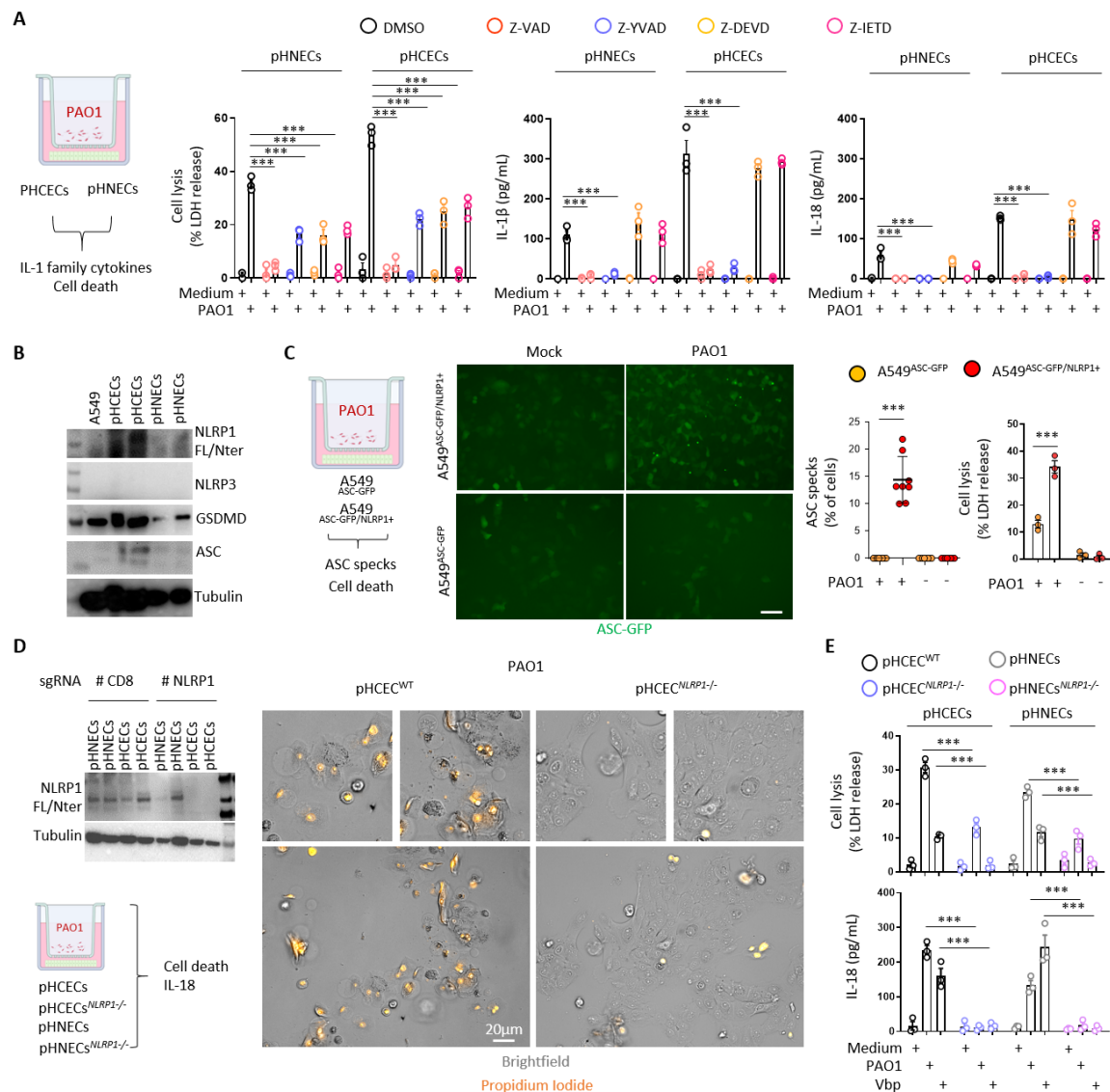


**Figure 1. *P. aeruginosa* triggers human NLRP1 inflammasome activation in corneal and nasal epithelial cells.**

A. Cell lysis (LDH) and IL-1 $\beta$ /IL-18 release evaluation in primary Human Corneal and Nasal Epithelial Cells, respectively pHCECs and pHNECs, upon *P. aeruginosa* (PAO1, 1.10<sup>5</sup> bacteria) co-culture for 24 hours. \*\*\*p  $\leq$  0.001, Two-Way Anova with multiple comparisons. Values are expressed as mean  $\pm$  SEM.

B. Immunoblotting examination of NLRP1, NLRP3, GSDMD, ASC and Tubulin in pHCECs and pHNECs. Immunoblots show lysates from one experiment performed three times.

C. Florescence microscopy and associated quantifications of ASC-GFP specks in A549<sup>NLRP1+/ASC-GFP</sup> and A549<sup>NLRP1-/ASC-GFP</sup> reporter cell lines exposed to *P. aeruginosa* (PAO1, 1.10<sup>5</sup> bacteria) for 24 hours. ASC-GFP (Green) pictures were taken in dish during after infection. Images shown are from one experiment and are representative of n = 8 independent experiments; scale bars, 50 µm. ASC complex percentage was performed by determining the ratios of cells positives for ASC speckles on the total cells (brightfield). At least 10 fields from each experiment were analyzed. Values are expressed as mean ± SEM. \*\*\*p ≤ 0.001, One-Way Anova.

D. Immunoblotting characterization of genetic invalidation of *NLRP1* in pHCECs and pHNECs population using CRISPR-Cas9 and microscopy visualization of plasma membrane permeabilization (Propidium Iodide incorporation, orange) in pHCECs co-cultured with PAO1 (1.10<sup>5</sup> bacteria) for 24 hours. Images shown are from one experiment and are representative of n = 3 independent experiments; scale bars, 20 µm.

E. Cell lysis (LDH) and IL-18 release evaluation in WT or *NLRP1*-deficient pHCECs and pHNECs, upon Valborono pro, Vbp 15µM) treatment or *P. aeruginosa* (PAO1, 1.10<sup>5</sup> bacteria) co-culture for 24 hours. \*\*\*p ≤ 0.001, Two-Way Anova with multiple comparisons. Values are expressed as mean ± SEM.



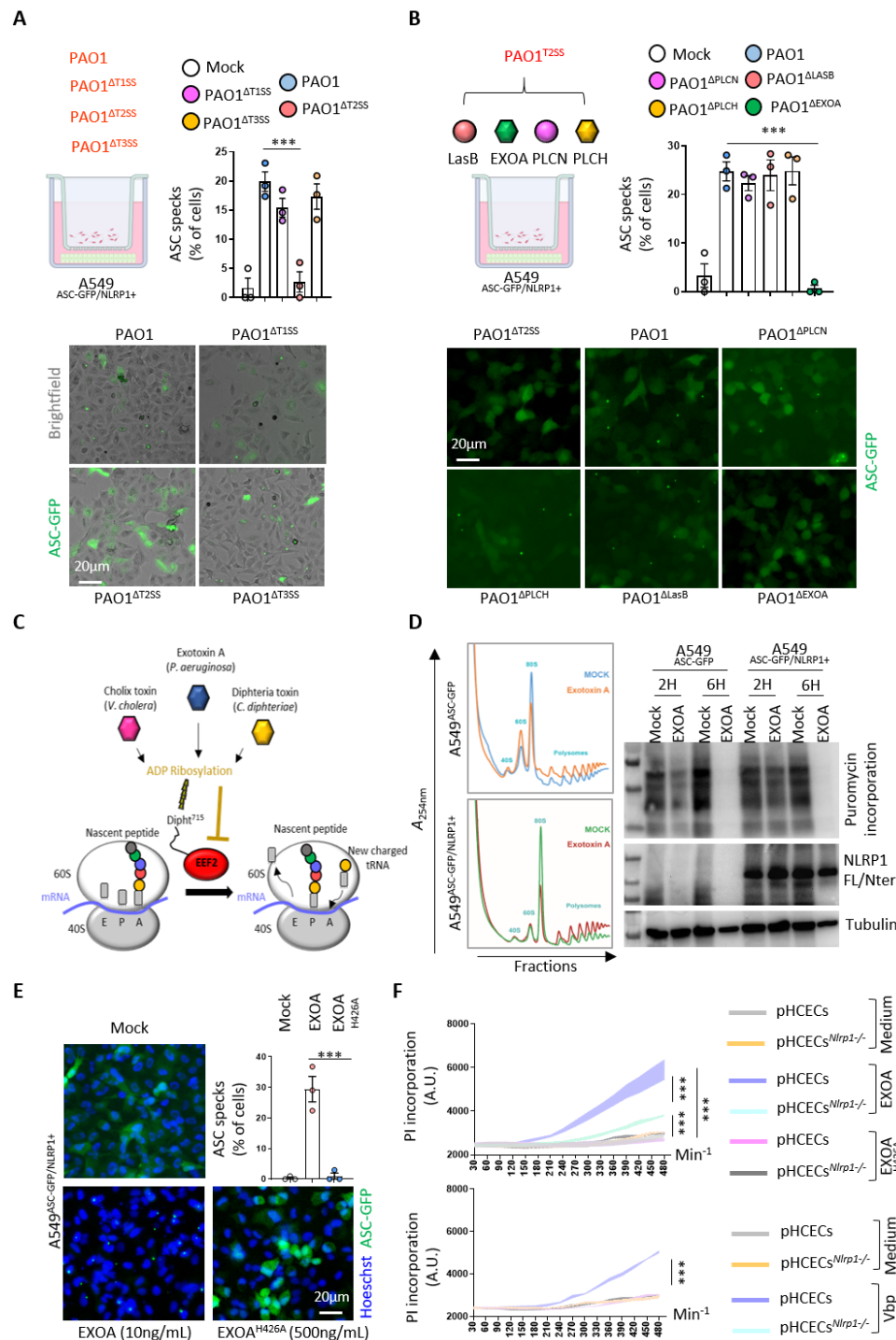


**Figure 2. *P. aeruginosa* EEF2-inactivating Exotoxin A (EXOA) promotes NLRP1 inflammasome response**

A. Fluorescence microscopy and associated quantifications of ASC-GFP specks in A549<sup>NLRP1+/ASC-GFP</sup> reporter cell lines exposed to 1.10<sup>5</sup> *P. aeruginosa* (PAO1) and



associated isogenic mutants for various Secretion Systems (PAO1<sup>ΔT3SS</sup>, PAO1<sup>ΔT2SS</sup>, PAO1<sup>ΔT1SS</sup>) for 24 hours. ASC-GFP (Green) pictures were taken in dish during after infection. Images shown are from one experiment and are representative of n = 3 independent experiments; scale bars, 20 μm. ASC complex percentage was performed by determining the ratios of cells positives for ASC speckles on the total cells (brightfield). At least 10 fields from n = 3 independent experiments were analyzed. Values are expressed as mean ± SEM. One-Way Anova.

B. Florescence microscopy and associated quantifications of ASC-GFP specks in A549<sup>NLRP1+/ASC-GFP</sup> reporter cell lines exposed to 1.10<sup>5</sup> *P. aeruginosa* (PAO1) and associated isogenic mutants for various Type-2 Secretion System virulence effectors (PAO1<sup>ΔPLCN</sup>, PAO1<sup>ΔPLCH</sup>, PAO1<sup>ΔLASB</sup>, PAO1<sup>ΔEXO A</sup>) for 24 hours. ASC-GFP (Green) pictures were taken in dish during after infection. Images shown are from one experiment and are representative of n = 3 independent experiments; scale bars, 20 μm. ASC complex percentage was performed by determining the ratios of cells positives for ASC speckles on the total cells (brightfield). At least 10 fields from n = 3 independent experiments were analyzed. Values are expressed as mean ± SEM. \*\*\*p ≤ 0.001, One-Way Anova.

C. Schematic mechanism of *P. aeruginosa* Exotoxin A (EXOA) and related toxins at mediating EEF2 ribosylation and inactivation and subsequent ribosome inactivation.

D. Determination of ribosome inactivation in A549<sup>NLRP1+/ASC-GFP</sup> and A549<sup>NLRP1-/ASC-GFP</sup> reporter cell lines exposed to Exotoxin A (EXOA, 10ng/mL) for 2 and 6 hours by measuring ribosome polysome accumulation and puromycin incorporation.

E. Florescence microscopy and associated quantifications of ASC-GFP specks in A549<sup>NLRP1+/ASC-GFP</sup> reporter cell lines exposed to EXOA (10ng/mL) or its catalytically dead mutant EXOA<sup>H426A</sup> (500ng/mL) for 10 hours. ASC-GFP (Green) pictures were taken in dish during after toxin exposure. Images shown are from one experiment and are representative of n = 3 independent experiments; scale bars, 20 μm. ASC complex percentage was performed by determining the ratios of cells positives for ASC speckles (Green, GFP) on the total nuclei (Blue, Hoechst). At least 10 fields from n = 3 independent experiments were analyzed. Values are expressed as mean ± SEM. \*\*\*p ≤ 0.001, One-Way Anova.

F. Plasma membrane permeabilization determination over time using Propidium Iodide (PI) incorporation in WT or NLRP1-deficient pHCECs exposed to Valboro (Vbp, 15μM), EXOA (10ng/mL) or EXOA<sup>H426A</sup> (10ng/mL) for indicated times. \*\*\*p ≤ 0.001, T-test. Values are expressed as mean ± SEM from one experiment (in triplicate) performed at least three times.

32

B. Cell lysis (LDH release), fluorescence microscopy and associated quantifications of ASC-GFP specks in A549<sup>NLRP1+/ASC-GFP</sup> and A549<sup>NLRP1+/ASC-GFP/ZAKα-</sup> reporter cell lines exposed to EXOA (10ng/mL) for 10 hours. ASC-GFP (Green) pictures were taken in dish during after toxin exposure. Images shown are from one experiment and are representative of n = 3 independent experiments; scale bars, 50 μm. ASC complex percentage was performed by determining the ratios of cells positives for ASC speckles (Green, GFP) on the total nuclei (Blue, Hoechst). At least 10 fields from n = 3 independent experiments were analyzed. Values are expressed as mean ± SEM. \*\*\*p ≤ 0.001, One-Way Anova.

C. Cell lysis (LDH release), fluorescence microscopy and associated quantifications of ASC-GFP specks in A549<sup>NLRP1+/ASC-GFP</sup> and A549<sup>NLRP1+/ASC-GFP/P38α/β-</sup> reporter cell lines exposed to EXOA (10ng/mL) for 10 hours. ASC-GFP (Green) pictures were taken in dish during after toxin exposure. Images shown are from one experiment and are representative of n = 3 independent experiments; scale bars, 50 μm. ASC complex percentage was performed by determining the ratios of cells positives for ASC speckles (Green, GFP) on the total cells (brightfield). At least 10 fields from n = 3 independent experiments were analyzed. Values are expressed as mean ± SEM. \*\*\*p ≤ 0.001, One-Way Anova.

D. Western blot examination of NLRP1 using an anti-NLRP1 N-terminal antibody (aa 1–323) in A549<sup>ASC-GFP</sup> reporter cells reconstituted with hNLRP1 or hNLRP1 plasmid constructs mutated for <sup>112</sup>TST<sup>114/112</sup>AAA<sup>114</sup> or <sup>178</sup>TST<sup>180/178</sup>AAA<sup>180</sup> after 10 hours exposure to EXOA (10ng/mL) or Vbp (15μM).

E. Cell lysis (LDH release), fluorescence microscopy and associated quantifications of ASC-GFP specks in A549<sup>ASC-GFP</sup> reporter cells reconstituted with hNLRP1 or hNLRP1 plasmid constructs mutated for <sup>112</sup>TST<sup>114/112</sup>AAA<sup>114</sup> or <sup>178</sup>TST<sup>180/178</sup>AAA<sup>180</sup> after 10 hours exposure to EXOA (10ng/mL) or Vbp (15μM). ASC-GFP (Green) pictures were taken in dish during after toxin exposure. Images shown are from one experiment and are representative of n = 3 independent experiments; scale bars, 50 μm. ASC complex percentage was performed by determining the ratios of cells positives for ASC speckles (Green, GFP) on the total cells (brightfield). At least 10 fields from n = 3 independent

experiments were analyzed. Values are expressed as mean  $\pm$  SEM. \*\*\* $p \leq 0.001$ , Two-Way Anova with multiple comparisons.

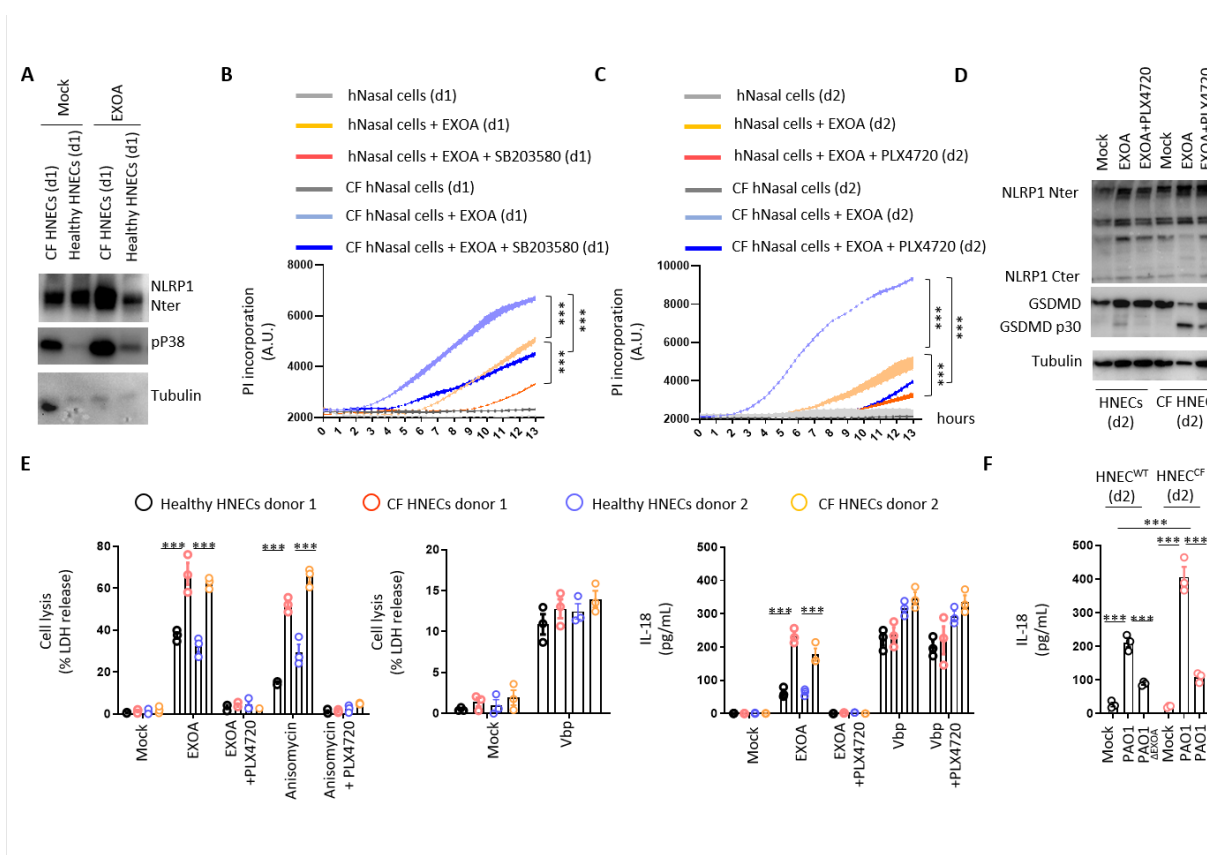


**Figure 4. Cystic fibrosis airway epithelial cells show exacerbated sensitivity to EXOA-driven pyroptosis, which is reversed by ZAKα inhibition.**

A. Immunoblotting of NLRP1, Tubulin and phosphorylated P38 in pHNECs<sup>WT</sup> and pHNECs<sup>CF</sup> from healthy (WT) and Cystic Fibrosis (CF) patients exposed to EXOA (10ng/mL) or not for 12 hours. Immunoblots show lysates from one experiment performed at least three times. (d1) stands for “donor 1” from Cystic fibrosis (CF) or healthy (WT) patients.

B, C. Plasma membrane permeabilization determination over time using Propidium Iodide (PI) incorporation in pHNECs<sup>WT</sup> or pHNECs<sup>CF</sup> exposed to EXOA (10ng/mL) for indicated times. When specified, SB203580, inhibitor of P38 activity (10μM) or PLX420 (bRaf, ZAKα inhibitor, 10μM) were used. (d1) and (d2) stand for respective donors 1 or 2. \*\*\*p ≤ 0.001, T-test. Values are expressed as mean ± SEM from one experiment (in triplicate) from one independent donor (d1/d2, CFd1/CFd2) performed at least three times.

D. Immunoblotting of NLRP1, Gasdermin D (GSDMD) and Tubulin in pHNECs<sup>WT</sup> and pHNECs<sup>CF</sup> from healthy (WT) and Cystic Fibrosis (CF) patients exposed to EXOA

(10ng/mL) or not for 12 hours in presence or absence of PLX420 (ZAK $\alpha$  inhibitor, 10 $\mu$ M). Immunoblots show combined supernatants and lysates from one experiment performed at least three times. (d2) stands for “donor 2” from Cystic fibrosis (CF) or healthy (WT) patients.

E. Cell lysis (LDH) and IL-18 release evaluation in pHNECs<sup>WT</sup> and pHNECs<sup>CF</sup> upon EXOA (10ng/mL), Anisomycin (1 $\mu$ g/mL) or Vbp (15 $\mu$ M) treatment for 18 hours in presence/absence of PLX420 (ZAK inhibitor, 10 $\mu$ M). \*\*\* $p \leq 0.001$ , T-test. Values are expressed as mean  $\pm$  SEM from one experiment (in triplicate) from one independent donor (d1/d2, CFd1/CFd2) performed at least three times.

F. IL-18 release in pHNECs<sup>WT</sup> and pHNECs<sup>CF</sup> co-cultured with PAO1 or PAO1 $\Delta$ EXOA (1.10<sup>5</sup> bacteria) for 24 hours. \*\*\* $p \leq 0.001$ , T-test. Values are expressed as mean  $\pm$  SEM from one experiment (in triplicate) from one independent donor (d2, CFd2) performed at least three times.



# SUPPLEMENTAL FIGURE LEGENDS

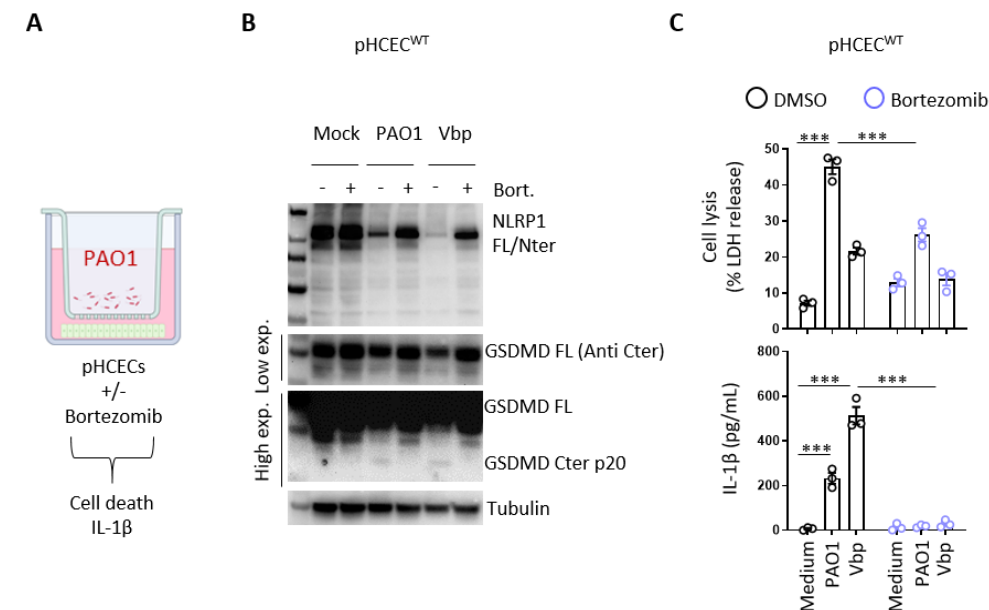


**Figure S1. *P. aeruginosa*-activated human NLRP1 inflammasome requires proteasome activity.**

A. Schematic drawing of *P. aeruginosa* co-culture experiments performed with human corneal epithelial cells.

B. Immunoblotting of NLRP1, Gasdermin-D and Tubulin in pHCECs upon Valbororo pro, Vbp 15μM) treatment or *P. aeruginosa* (PAO1, 1.10<sup>5</sup> bacteria) co-culture for 24 hours in presence/absence of proteasome inhibitor bortezomib. Immunoblots show lysates from one experiment performed at least three times.

C. Cell lysis (LDH) and IL-1B release evaluation in pHCECs and pHNECs, upon Valbororo pro, Vbp 15μM) treatment or *P. aeruginosa* (PAO1, 1.10<sup>5</sup> bacteria) co-culture for 24 hours in presence/absence of proteasome inhibitor bortezomib. \*\*\*p ≤ 0.001, Two-Way Anova with multiple comparisons. Values are expressed as mean ± SEM.

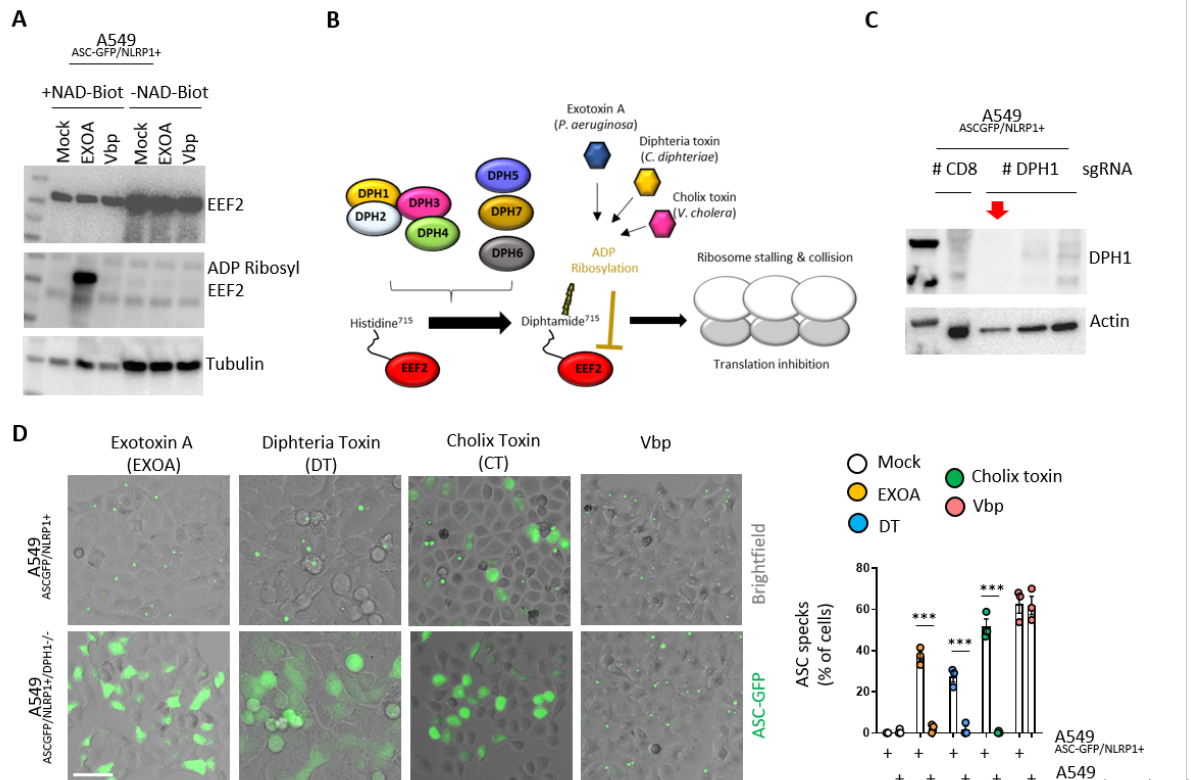


**Figure S2. Multiple EEF2-targeting toxins activate the human NLRP1 inflammasome.**

B. Immunoblotting of ADP-Ribosylated proteins, EEF2 and Tubulin in A549<sup>NLRP1+/ASC-GFP</sup> cell lysates treated or not with Vbp (15μM) or EXOA (10ng/mL) in presence of NAD-Biot. Immunoblots show lysates from one experiment performed at least three times.

B. Schematic mechanism of DPH enzymes at promoting the formation of the Dipthamide aminoacid on EEF2.

C. Immunoblotting characterization of genetic invalidation of *DPH1* in A549<sup>NLRP1+/ASC-GFP</sup> cells using CRISPR-Cas9.

D. Fluorescence microscopy and associated quantifications of ASC-GFP specks in A549<sup>NLRP1+/ASC-GFP</sup> and A549<sup>NLRP1+/ASC-GFP/DPH1<sup>-/-</sup></sup> reporter cell lines exposed to Vbp (15μM), EXOA (10ng/mL), Cholix Toxin (CT, 10ng/mL) and Diphtheria Toxin (DT, 20ng/mL) for 10 hours. ASC-GFP (Green) pictures were taken in dish during after toxin exposure. Images shown are from one experiment and are representative of n = 3 independent experiments; scale bars, 50 μm. ASC complex percentage was performed by determining the ratios of cells positives for ASC speckles (Green, GFP) on the total cells (Brightfield). At least 10

fields from n = 3 independent experiments were analyzed. Values are expressed as mean  
 $\pm$  SEM. \*\*\*p  $\leq$  0.001, One-Way Anova.

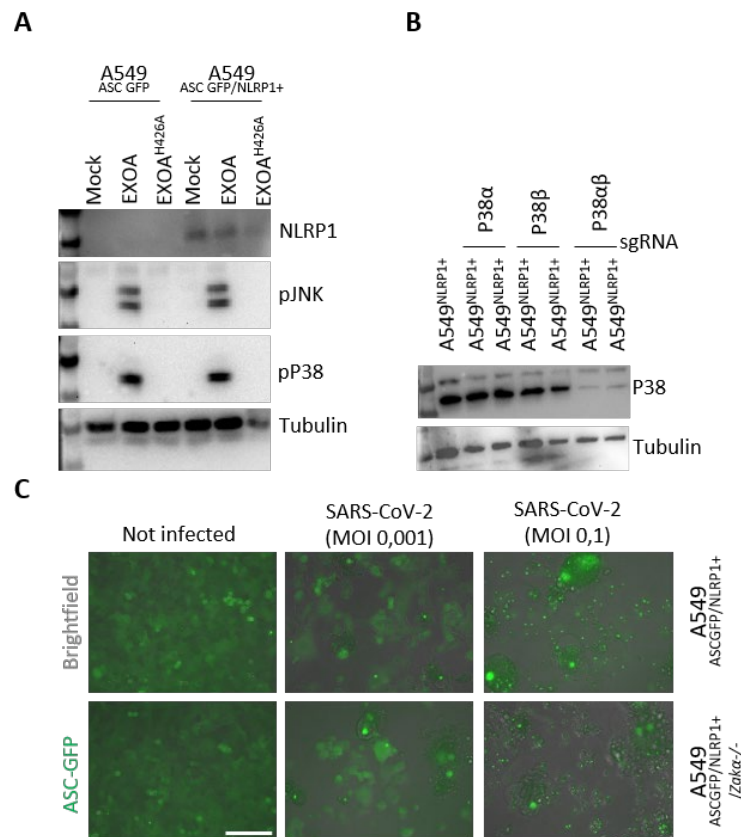


**Figure S3. Stress kinase ZAK $\alpha$  regulates EXOA-, but not SARS-CoV-2-driven NLRP1 inflammasome activation.**

A. Immunoblotting of NLRP1, Tubulin and phosphorylated P38 and JNK in A549<sup>NLRP1+</sup> and A549<sup>NLRP1-</sup> reporter cell lines exposed or not to EXOA (10ng/mL) or its inactive mutant EXOA<sup>H426A</sup> for 3 hours. Immunoblots show lysates from one experiment performed at least three times.

B. Immunoblotting characterization of genetic invalidation of *P38 $\alpha$*  and *P38 $\beta$*  in A549<sup>NLRP1+/ASC-GFP</sup> cells using CRISPR-Cas9.

C. Fluorescence microscopy and associated quantifications of ASC-GFP specks in A549<sup>NLRP1+/ASC-GFP</sup> and A549<sup>NLRP1+/ASC-GFP/ZAK $\alpha$ -</sup> reporter cell lines expressing hACE2 infected for 24 hours with various SARS-CoV-2 MOI (Multiplicity of infection). ASC-GFP (Green) pictures were taken in dish during after toxin exposure. Images shown are from one experiment and are representative of n = 3 independent experiments; scale bars, 50  $\mu$ m. ASC complex percentage was performed by determining the ratios of cells positives for ASC speckles (Green, GFP) on the total cells (Brightfield).

**A**

**# CF03 (donor 1)**

Sex: Male  
Age: 28  
Disease: Cystic Fibrosis  
Mutation:  $\Delta F508$  / 4005+1G>A  
Date of Nasal swab: 09/05/2022

**# CF06 (donor 2)**

Sex: Male  
Age: 34  
Disease: Cystic Fibrosis  
Mutation:  $\Delta F508$  / N1303K  
Date of Nasal swab: 21/06/2022

**# H1 (donor 1)**

Sex: Male  
Age: 29  
Disease: None  
Mutation: None  
Date of Nasal swab: 09/05/2022

**# H2 (donor 2)**

Sex: Female  
Age: 23  
Disease: None  
Mutation: None  
Date of Nasal swab: 20/06/2022

**B**

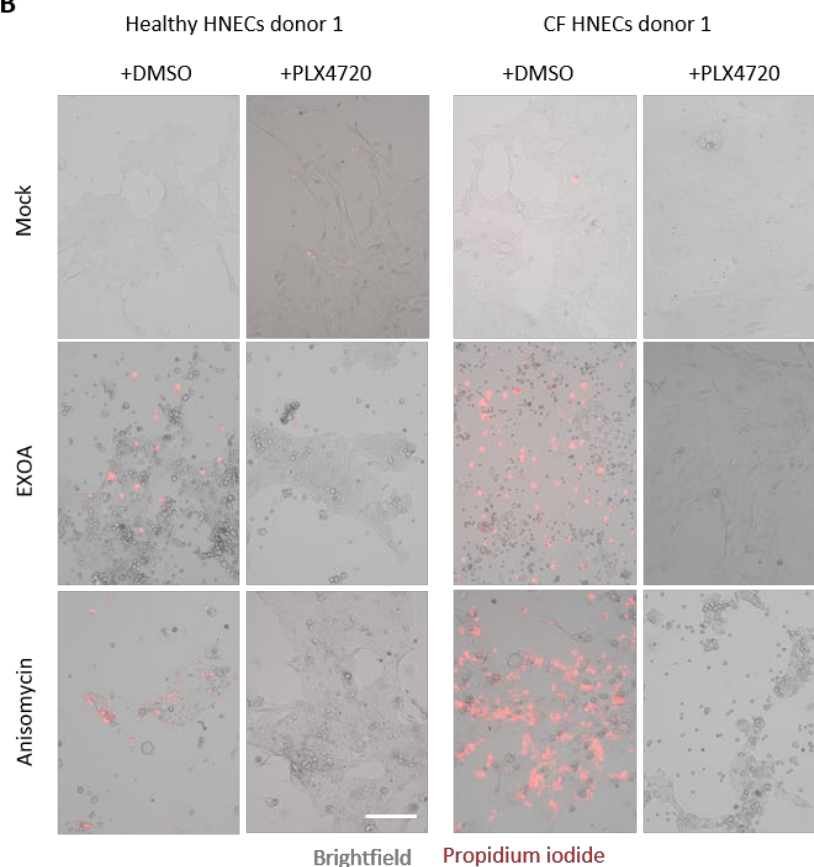


**Figure S4. Cystic fibrosis (CF) cells show exacerbated sensitivity to undergo cell death upon ribotoxic stress.**

A. Information regarding Healthy and CF patient samples used in this study.

B. Fluorescence microscopy of Propidium Iodide (PI, red) incorporation into pHNEC<sup>WT</sup> (donor 2, d2) and pHNEC<sup>CF</sup> (donor 1, d1) after exposure to Anisomycin or EXOA for 16

hours in presence or not of the ZAK alpha inhibitor PLX4720 (10μM). Images shown are from one experiment and are representative of n = 3 independent experiments; scale bars, 50 μm.

# REFERENCES

- Allison, A.C. 1954. Protection Afforded by Sick-cell Trait Against Subtertian Malarial Infection. *Br. Med. J.* 1:290. doi:10.1136/BMJ.1.4857.290.
- Armstrong, S., and A.R. Merrill. 2004. Toward the Elucidation of the Catalytic Mechanism of the Mono-ADP-Ribosyltransferase Activity of *Pseudomonas aeruginosa* Exotoxin A. *Biochemistry*. 43:183–194. doi:10.1021/bi034772u.
- Balakrishnan, A., R. Karki, B. Berwin, M. Yamamoto, and T.D. Kanneganti. 2018. Guanylate binding proteins facilitate caspase-11-dependent pyroptosis in response to type 3 secretion system-negative *Pseudomonas aeruginosa*. *Cell Death Discov.* 4:1–12. doi:10.1038/S41420-018-0068-Z.
- Bauernfried, S., M.J. Scherr, A. Pichlmair, K.E. Duderstadt, and V. Hornung. 2021. Human NLRP1 is a sensor for double-stranded RNA. *Science*. 371. doi:10.1126/SCIENCE.ABD0811.
- Bérubé, J., L. Roussel, L. Nattagh, and S. Rousseau. 2010. Loss of Cystic Fibrosis Transmembrane Conductance Regulator Function Enhances Activation of P38 and ERK MAPKs, Increasing Interleukin-6 Synthesis in Airway Epithelial Cells Exposed to *Pseudomonas aeruginosa*. *J. Biol. Chem.* 285:22299–22307. doi:10.1074/JBC.M109.098566.
- Bonfield, T.L., J.R. Panuska, M.W. Konstan, K.A. Hilliard, J.B. Hilliard, H. Ghnaim, and M. Berger. 2012. Inflammatory cytokines in cystic fibrosis lungs. <https://doi.org/10.1164/ajrccm.152.6.8520783>. 152:2111–2118. doi:10.1164/AJRCCM.152.6.8520783.
- Broz, P., and V.M. Dixit. 2016. Inflammasomes: mechanism of assembly, regulation and signalling. *Nat. Rev. Immunol.* 2016 167. 16:407–420. doi:10.1038/nri.2016.58.
- Chen, Y., X. Shao, J. Cao, H. Zhu, B. Yang, Q. He, and M. Ying. 2021. Phosphorylation regulates cullin-based ubiquitination in tumorigenesis. *Acta Pharm. Sin. B.* 11:309. doi:10.1016/J.APSB.2020.09.007.
- Deng, Q., Y. Wang, Y. Zhang, M. Li, D. Li, X. Huang, Y. Wu, J. Pu, and M. Wu. 2015. *Pseudomonas aeruginosa* Triggers Macrophage Autophagy To Escape Intracellular Killing by Activation of the NLRP3 Inflammasome. *Infect. Immun.* 84:56–66. doi:10.1128/IAI.00945-15.



1019 Faure, E., J.B. Mear, K. Faure, S. Normand, A. Couturier-Maillard, T. Grandjean, V.  
1020 Balloy, B. Ryffel, R. Dessein, M. Chignard, C. Uyttenhove, B. Guery, P. Gosset, M.  
1021 Chamaillard, and E. Kipnis. 2014. Pseudomonas aeruginosa type-3 secretion  
1022 system dampens host defense by exploiting the NLRC4-coupled inflammasome.  
1023 *Am. J. Respir. Crit. Care Med.* 189:799–811. doi:10.1164/RCCM.201307-1358OC.  
1024 Fenini, G., S. Grossi, E. Contassot, T. Biedermann, E. Reichmann, L.E. French, and  
1025 H.D. Beer. 2018. Genome Editing of Human Primary Keratinocytes by  
1026 CRISPR/Cas9 Reveals an Essential Role of the NLRP1 Inflammasome in UVB  
1027 Sensing. *J. Invest. Dermatol.* 138:2644–2652. doi:10.1016/J.JID.2018.07.016.  
1028 Filloux, A. 2011. Protein Secretion Systems in Pseudomonas aeruginosa: An Essay on  
1029 Diversity, Evolution, and Function. *Front. Microbiol.* 2.  
1030 doi:10.3389/FMICB.2011.00155.  
1031 Filloux, A. 2022. Bacterial protein secretion systems: Game of types. *Microbiol. (United*  
1032 *Kingdom)*. 168:001193. doi:10.1099/MIC.0.001193/CITE/REFWORKS.  
1033 Franchi, L., J. Stoolman, T.D. Kanneganti, A. Verma, R. Ramphal, and G. Núñez. 2007.  
1034 Critical role for Ipaf in Pseudomonas aeruginosa-induced caspase-1 activation. *Eur.*  
1035 *J. Immunol.* 37:3030–3039. doi:10.1002/EJI.200737532.  
1036 Griswold, A.R., H.C. Huang, and D.A. Bachovchin. 2022. The NLRP1 Inflammasome  
1037 Induces Pyroptosis in Human Corneal Epithelial Cells. *Invest. Ophthalmol. Vis. Sci.*  
1038 63. doi:10.1167/IOVS.63.3.2.  
1039 Hawer, H., B.A. Mendelsohn, K. Mayer, A. Kung, A. Malhotra, S. Tuupainen, J. Schleit,  
1040 U. Brinkmann, and R. Schaffrath. 2020. Diphthamide-deficiency syndrome: a novel  
1041 human developmental disorder and ribosomopathy. *Eur. J. Hum. Genet.* 2020  
1042 2811. 28:1497–1508. doi:10.1038/s41431-020-0668-y.  
1043 Hazlett, L.D. 2005. Inflammatory Response to Pseudomonas aeruginosa Keratitis. *Ocul.*  
1044 *Surf.* 3:S-139. doi:10.1016/S1542-0124(12)70239-2.  
1045 Ivankovic, M., I. Rubelj, M. Matulic, E. Reich, and B. Brdar. 2006. Site-specific  
1046 mutagenesis of the histidine precursor of diphthamide in the human elongation  
1047 factor-2 gene confers resistance to diphtheria toxin. *Mutat. Res. Toxicol. Environ.*  
1048 *Mutagen.* 609:34–42. doi:10.1016/J.MRGENTOX.2006.06.027.  
1049 Jacobs, M.A., A. Alwood, I. Thaipisuttikul, D. Spencer, E. Haugen, S. Ernst, O. Will, R.

Kaul, C. Raymond, R. Levy, L. Chun-Rong, D. Guenther, D. Bovee, M. V. Olson, and C. Manoil. 2003. Comprehensive transposon mutant library of *Pseudomonas aeruginosa*. *Proc. Natl. Acad. Sci. U. S. A.* 100:14339–14344. doi:10.1073/PNAS.2036282100/SUPPL\_FILE/6282TABLE6.HTML.

Jenster, L.-M., K.-E. Lange, S. Normann, A. vom Hemdt, J.D. Wuerth, L.D.J. Schiffelers, Y.M. Tesfamariam, F.N. Gohr, L. Klein, I.H. Kaltheuner, S. Ebner, D.J. Lapp, J. Mayer, J. Moecking, H.L. Ploegh, E. Latz, F. Meissner, M. Geyer, B.M. Kümmerer, and F.I. Schmidt. 2023. P38 kinases mediate NLRP1 inflammasome activation after ribotoxic stress response and virus infection. *J. Exp. Med.* 220. doi:10.1084/JEM.20220837.

Jørgensen, R., A.R. Merrill, S.P. Yates, V.E. Marquez, A.L. Schwan, T. Boesen, and G.R. Andersen. 2005. Exotoxin A-eEF2 complex structure indicates ADP ribosylation by ribosome mimicry. *Nature*. 436:979–984. doi:10.1038/NATURE03871.

Jørgensen, R., A.E. Purdy, R.J. Fieldhouse, M.S. Kimber, D.H. Bartlett, and A.R. Merrill. 2008. Cholix toxin, a novel ADP-ribosylating factor from *Vibrio cholerae*. *J. Biol. Chem.* 283:10671–10678. doi:10.1074/JBC.M710008200.

Kaftrio | European Medicines Agency.

Kayagaki, N., O.S. Kornfeld, B.L. Lee, I.B. Stowe, K. O’Rourke, Q. Li, W. Sandoval, D. Yan, J. Kang, M. Xu, J. Zhang, W.P. Lee, B.S. McKenzie, G. Ulas, J. Payandeh, M. Roose-Girma, Z. Modrusan, R. Reja, M. Sagolla, J.D. Webster, V. Cho, T.D. Andrews, L.X. Morris, L.A. Miosge, C.C. Goodnow, E.M. Bertram, and V.M. Dixit. 2021. NINJ1 mediates plasma membrane rupture during lytic cell death. *Nature*. 591:131–136. doi:10.1038/S41586-021-03218-7.

Lacey, C.A., and E.A. Miao. 2020. Programmed Cell Death in the Evolutionary Race against Bacterial Virulence Factors. *Cold Spring Harb. Perspect. Biol.* 12. doi:10.1101/CSHPERSPECT.A036459.

Liao, C., X. Huang, Q. Wang, D. Yao, and W. Lu. 2022. Virulence Factors of *Pseudomonas Aeruginosa* and Antivirulence Strategies to Combat Its Drug Resistance. *Front. Cell. Infect. Microbiol.* 12:918. doi:10.3389/FCIMB.2022.926758/BIBTEX.

- 1081 Liu, S., G.T. Milne, J.G. Kuremsky, G.R. Fink, and S.H. Leppla. 2004. Identification of  
1082 the Proteins Required for Biosynthesis of Diphthamide, the Target of Bacterial  
1083 ADP-Ribosylating Toxins on Translation Elongation Factor 2. *Mol. Cell. Biol.*  
1084 24:9487. doi:10.1128/MCB.24.21.9487-9497.2004.
- 1085 Maurice, N.M., B. Bedi, and R.T. Sadikot. 2018. Pseudomonas aeruginosa biofilms:  
1086 Host response and clinical implications in lung infections. *Am. J. Respir. Cell Mol.*  
1087 *Biol.* 58:428–439. doi:10.1165/RCMB.2017-  
1088 0321TR/SUPPL\_FILE/DISCLOSURES.PDF.
- 1089 Miao, E.A., R.K. Ernst, M. Dors, D.P. Mao, and A. Aderem. 2008. Pseudomonas  
1090 aeruginosa activates caspase 1 through Ipaf. *Proc. Natl. Acad. Sci. U. S. A.*  
1091 105:2562–2567. doi:10.1073/PNAS.0712183105/ASSET/BDFA0AA1-5368-45F0-  
1092 B680-77545D4B3F8B/ASSETS/GRAPHIC/ZPQ0050893430006.JPEG.
- 1093 Michalska, M., and P. Wolf. 2015. Pseudomonas Exotoxin A: Optimized by evolution for  
1094 effective killing. *Front. Microbiol.* 6:963. doi:10.3389/FMICB.2015.00963/BIBTEX.
- 1095 Nakajima, J., S. Oana, T. Sakaguchi, M. Nakashima, H. Numabe, H. Kawashima, N.  
1096 Matsumoto, and N. Miyake. 2018. Novel compound heterozygous DPH1 mutations  
1097 in a patient with the unique clinical features of airway obstruction and external  
1098 genital abnormalities. *J. Hum. Genet.* 63:529–532. doi:10.1038/S10038-017-0399-  
1099 2.
- 1100 Ogura, K., K. Yahiro, H. Tsutsuki, S. Nagasawa, S. Yamasaki, J. Moss, and M. Noda.  
1101 2011. Characterization of Cholix toxin-induced apoptosis in HeLa cells. *J. Biol.*  
1102 *Chem.* 286:37207–37215. doi:10.1074/JBC.M111.246504.
- 1103 De Oliveira, D.M.P., B.M. Forde, T.J. Kidd, P.N.A. Harris, M.A. Schembri, S.A. Beatson,  
1104 D.L. Paterson, and M.J. Walker. 2020. Antimicrobial resistance in ESKAPE  
1105 pathogens. *Clin. Microbiol. Rev.* 33. doi:10.1128/CMR.00181-  
1106 19/ASSET/CBA1C1D1-CF90-43DE-A9DF-  
1107 32D24A4334AC/ASSETS/GRAPHIC/CMR.00181-19-F0001.JPEG.
- 1108 Park, Y.H., E.F. Remmers, W. Lee, A.K. Ombrello, L.K. Chung, Z. Shilei, D.L. Stone,  
1109 M.I. Ivanov, N.A. Loeven, K.S. Barron, P. Hoffmann, M. Nehrebecky, Y.Z. Akkaya-  
1110 Ulum, E. Sag, B. Balci-Peynircioglu, I. Aksentijevich, A. Gül, C.N. Rotimi, H. Chen,  
1111 J.B. Bliska, S. Ozen, D.L. Kastner, D. Shriner, and J.J. Chae. 2020. Ancient familial

1112 Mediterranean fever mutations in human pyrin and resistance to *Yersinia pestis*.  
1113 *Nat. Immunol.* 21:857–867. doi:10.1038/S41590-020-0705-6.

1114 Pillar, C.M., and J.A. Hobden. 2002. *Pseudomonas aeruginosa* exotoxin A and keratitis  
1115 in mice. *Invest. Ophthalmol. Vis. Sci.* 43:1437–1444.

1116 Planès, R., M. Pinilla, K. Santoni, A. Hessel, C. Passemar, K. Lay, P. Paillette, A.L.C.  
1117 Valadão, K.S. Robinson, P. Bastard, N. Lam, R. Fadrique, I. Rossi, D. Pericat, S.  
1118 Bagayoko, S.A. Leon-Icaza, Y. Rombouts, E. Perouzel, M. Tiraby, Q. Zhang, P.  
1119 Cicuti, E. Jouanguy, O. Neyrolles, C.E. Bryant, A.R. Floto, C. Goujon, F.Z. Lei, G.  
1120 Martin-Blondel, S. Silva, J.L. Casanova, C. Cougoule, B. Reversade, J. Marcoux,  
1121 E. Ravet, and E. Meunier. 2022. Human NLRP1 is a sensor of pathogenic  
1122 coronavirus 3CL proteases in lung epithelial cells. *Mol. Cell.* 82:2385-2400.e9.  
1123 doi:10.1016/J.MOLCEL.2022.04.033.

1124 Qin, S., W. Xiao, C. Zhou, Q. Pu, X. Deng, L. Lan, H. Liang, X. Song, and M. Wu. 2022.  
1125 *Pseudomonas aeruginosa*: pathogenesis, virulence factors, antibiotic resistance,  
1126 interaction with host, technology advances and emerging therapeutics. *Signal*  
1127 *Transduct. Target. Ther.* 2022 71. 7:1–27. doi:10.1038/s41392-022-01056-1.

1128 Raia, V., L. Maiuri, C. Ciacchi, I. Ricciardelli, L. Vacca, S. Auricchio, M. Cimmino, M.  
1129 Cavaliere, M. Nardone, A. Cesaro, J. Malcolm, S. Quarantino, and M. Londei. 2005.  
1130 Inhibition of P38 mitogen activated protein kinase controls airway inflammation in  
1131 cystic fibrosis. *Thorax.* 60:773–780. doi:10.1136/THX.2005.042564.

1132 Roberts, T.M., and A.R. Merrill. 2002. A re-evaluation of the role of histidine-426 within  
1133 *Pseudomonas aeruginosa* exotoxin A. *Biochem. J.* 367:601–608.  
1134 doi:10.1042/BJ20020768.

1135 Robinson, K.S., D.E.T. Teo, K. Sen Tan, G.A. Toh, H.H. Ong, C.K. Lim, K. Lay, B.V. Au,  
1136 T.S. Lew, J.J.H. Chu, V.T.K. Chow, D.Y. Wang, F.L. Zhong, and B. Reversade.  
1137 2020. Enteroviral 3C protease activates the human NLRP1 inflammasome in  
1138 airway epithelia. *Science.* 370. doi:10.1126/SCIENCE.AAY2002.

1139 Robinson, K.S., G.A. Toh, P. Rozario, R. Chua, S. Bauernfried, Z. Sun, M.J. Firdaus, S.  
1140 Bayat, R. Nadkarni, Z.S. Poh, K.C. Tham, C.R. Harapas, C.K. Lim, W. Chu, C.W.S.  
1141 Tay, K.Y. Tan, T. Zhao, C. Bonnard, R. Sobota, J.E. Connolly, J. Common, S.L.  
1142 Masters, K.W. Chen, L. Ho, B. Wu, V. Hornung, and F.L. Zhong. 2022. ZAKα-

1143 driven ribotoxic stress response activates the human NLRP1 inflammasome.  
 1144 *Science*. 377:328–335. doi:10.1126/SCIENCE.ABL6324.

1145 Ryu, J.C., M.J. Kim, Y. Kwon, J.H. Oh, S.S. Yoon, S.J. Shin, J.H. Yoon, and J.H. Ryu.  
 1146 2016. Neutrophil pyroptosis mediates pathology of *P. aeruginosa* lung infection in  
 1147 the absence of the NADPH oxidase NOX2. *Mucosal Immunol.* 2017 103. 10:757–  
 1148 774. doi:10.1038/mi.2016.73.

1149 Samson, M., F. Libert, B.J. Doranz, J. Rucker, C. Liesnard, M. Farber, S. Saragosti, C.  
 1150 Lapoumeroulie, J. Cognaux, C. Forceille, G. Muyltermans, C. Verhofstede, G.  
 1151 Burtonboy, M. Georges, T. Imai, S. Rana, Y. Yi, R.J. Smyth, M. Parmentier, and al  
 1152 et. 1996. Resistance to HIV-1 infection in caucasian individuals bearing mutant  
 1153 alleles of the CCR-5 chemokine receptor gene. *Nature*. 382:722–726.  
 1154 doi:10.1038/382722A0.

1155 Santoni, K., D. Pericat, L. Gorse, J. Buyck, M. Pinilla, L. Prouvensier, S. Bagayoko, A.  
 1156 Hessel, S.A. Leon-Icaza, E. Bellard, S. Mazères, E. Doz-Deblauw, N. Winter, C.  
 1157 Paget, J.P. Girard, C.T.N. Pham, C. Cougoule, R. Poincloux, M. Lamkanfi, E.  
 1158 Lefrançais, E. Meunier, and R. Planès. 2022a. Caspase-1-driven neutrophil  
 1159 pyroptosis and its role in host susceptibility to *Pseudomonas aeruginosa*. *PLOS*  
 1160 *Pathog.* 18:e1010305. doi:10.1371/JOURNAL.PPAT.1010305.

1161 Santoni, K., D. Pericat, L. Gorse, J. Buyck, M. Pinilla, L. Prouvensier, S. Bagayoko, A.  
 1162 Hessel, S.A. Leon-Icaza, E. Bellard, S. Mazères, E. Doz-Deblauw, N. Winter, C.  
 1163 Paget, J.P. Girard, C.T.N. Pham, C. Cougoule, R. Poincloux, M. Lamkanfi, E.  
 1164 Lefrançais, E. Meunier, and R. Planès. 2022b. Caspase-1-driven neutrophil  
 1165 pyroptosis and its role in host susceptibility to *Pseudomonas aeruginosa*. *PLOS*  
 1166 *Pathog.* 18:e1010305. doi:10.1371/JOURNAL.PPAT.1010305.

1167 Spornovasilis, N., M. Psychogiou, and G. Poulakou. 2021. Skin manifestations of  
 1168 *Pseudomonas aeruginosa* infections. *Curr. Opin. Infect. Dis.* 34:72–79.  
 1169 doi:10.1097/QCO.0000000000000717.

1170 Sutterwala, F.S., L.A. Mijares, L. Li, Y. Ogura, B.I. Kazmierczak, and R.A. Flavell. 2007.  
 1171 Immune recognition of *Pseudomonas aeruginosa* mediated by the IPAF/NLRC4  
 1172 inflammasome. *J. Exp. Med.* 204:3235. doi:10.1084/JEM.20071239.

1173 Tsu, B. V., C. Beierschmitt, A.P. Ryan, R. Agarwal, P.S. Mitchell, and M.D. Daugherty.

2021. Diverse viral proteases activate the NLRP1 inflammasome. *Elife*. 10:1–76.  
doi:10.7554/ELIFE.60609.

Urreizti, R., K. Mayer, G.D. Evrony, E. Said, L. Castilla-Vallmanya, N.A.L. Cody, G. Plasencia, B.D. Gelb, D. Grinberg, U. Brinkmann, B.D. Webb, and S. Balcells. 2020. DPH1 syndrome: two novel variants and structural and functional analyses of seven missense variants identified in syndromic patients. *Eur. J. Hum. Genet.* 28:64–75. doi:10.1038/S41431-019-0374-9.

Veit, G., R.G. Avramescu, A.N. Chiang, S.A. Houck, Z. Cai, K.W. Peters, J.S. Hong, H.B. Pollard, W.B. Guggino, W.E. Balch, W.R. Skach, G.R. Cutting, R.A. Frizzell, D.N. Sheppard, D.M. Cyr, E.J. Sorscher, J.L. Brodsky, and G.L. Lukacs. 2016. From CFTR biology toward combinatorial pharmacotherapy: expanded classification of cystic fibrosis mutations. *Mol. Biol. Cell*. 27:424. doi:10.1091/MBC.E14-04-0935.

Vind, A.C., G. Snieckute, M. Blasius, C. Tiedje, N. Krogh, D.B. Bekker-Jensen, K.L. Andersen, C. Nordgaard, M.A.X. Tollenaere, A.H. Lund, J.V. Olsen, H. Nielsen, and S. Bekker-Jensen. 2020. ZAK $\alpha$  Recognizes Stalled Ribosomes through Partially Redundant Sensor Domains. *Mol. Cell*. 78:700–713. doi:10.1016/J.MOLCEL.2020.03.021.

Wu, C.C.C., A. Peterson, B. Zinshteyn, S. Regot, and R. Green. 2020. Ribosome Collisions Trigger General Stress Responses to Regulate Cell Fate. *Cell*. 182:404-416.e14. doi:10.1016/J.CELL.2020.06.006.

Zhong, F.L., O. Mamaï, L. Sborgi, L. Boussofara, R. Hopkins, K. Robinson, I. Szeverényi, T. Takeichi, R. Balaji, A. Lau, H. Tye, K. Roy, C. Bonnard, P.J. Ahl, L.A. Jones, P. Baker, L. Lacina, A. Otsuka, P.R. Fournie, F. Malecaze, E.B. Lane, M. Akiyama, K. Kabashima, J.E. Connolly, S.L. Masters, V.J. Soler, S.S. Omar, J.A. McGrath, R. Nedelcu, M. Gribaa, M. Denguezli, A. Saad, S. Hiller, and B. Reversade. 2016. Germline NLRP1 Mutations Cause Skin Inflammatory and Cancer Susceptibility Syndromes via Inflammasome Activation. *Cell*. 167:187-202.e17. doi:10.1016/J.CELL.2016.09.001.